iScience

CellPress
OPEN ACCESS

Article

RNA expression profiles and regulatory networks in human right ventricular hypertrophy due to high pressure load

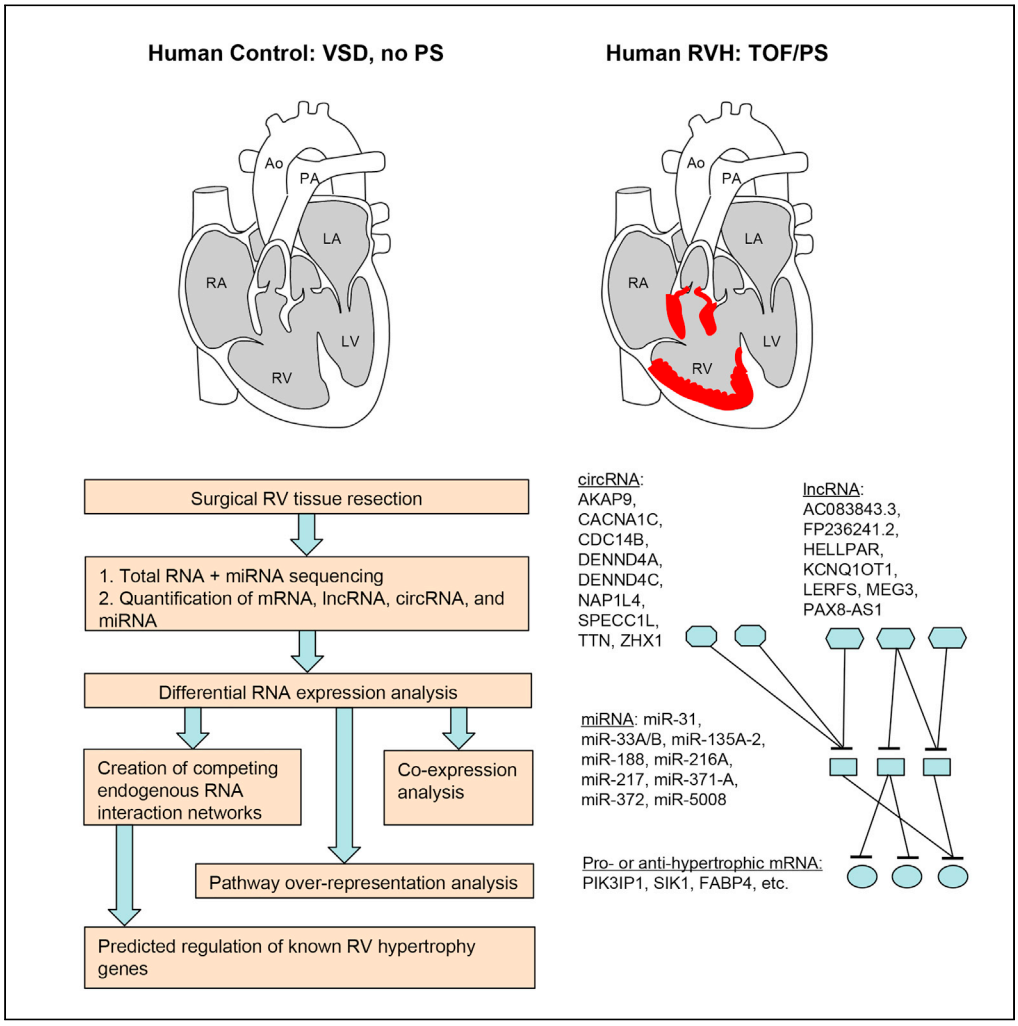

Philippe Chouvarine, Joachim Photiadis, Robert Cesnjevar, ..., Sven Dittrich, Felix Berger, Georg Hansmann

georg.hansmann@gmail.com

HIGHLIGHTS

First comprehensive transcriptomic study of human RVH via RNA expression and network analysis

First human RVH study using exclusively freshly isolated myocardium

Known hypertrophy genes are regulated the strongest by competing endogenous RNA networks in RVH

Epigenetic mRNA regulation in RVH by ncRNAs is dependent on sex and age

Chouvarine et al., iScience 24, 102232
March 19, 2021
https://doi.org/10.1016/j.isci.2021.102232

iScience

CellPress
OPEN ACCESS

Article

RNA expression profiles and regulatory networks in human right ventricular hypertrophy due to high pressure load

Philippe Chouvarine,[1] Joachim Photiadis,[2,5] Robert Cesnjevar,[3,5] Jens Scheewe,[4,5] Ulrike M.M. Bauer,[5,6] Thomas Pickardt,[5,6] Hans-Heiner Kramer,[4,5] Sven Dittrich,[3,5] Felix Berger,[2,5] and Georg Hansmann[1,5,7,*]

SUMMARY

Right ventricular hypertrophy (RVH) occurs in high pressure afterload, e.g., tetralogy of Fallot/pulmonary stenosis (TOF/PS). Such RVH is associated with alterations in energy metabolism, neurohormonal and epigenetic dysregulation (e.g., microRNA), and fetal gene reprogramming in animal models. However, comprehensive expression profiling of competing endogenous RNA in human RVH has not been performed. Here, we unravel several previously unknown circular, long non-coding, and microRNAs, predicted to regulate expression of genes specific to human RVH in the non-failing heart (TOF/PS). These genes are significantly overrepresented in pathways related to regulation of glucose and lipid metabolism (SIK1, FABP4), cell surface interactions (THBS2, FN1), apoptosis (PIK3IP1, SIK1), extracellular matrix composition (CTGF, IGF1), and other biological events. This is the first unbiased RNA sequencing study of human compensated RVH encompassing coding and non-coding RNA expression and predicted sponging of miRNAs by non-coding RNAs. These findings advance our understanding of adaptive RVH and highlight future therapeutic targets.

INTRODUCTION

Right ventricular hypertrophy (RVH) occurs in pulmonary hypertension (PH), tetralogy of Fallot/pulmonary stenosis (TOF/PS), or other conditions with high right ventricular (RV) pressure afterload. RV adaptation and remodeling in high pressure afterload involves a number of interdependent complex processes, such as altered bioenergetics (hypoxia/ischemia and mitochondrial remodeling/dysfunction) and neurohormonal and immunological activation. In concert with underlying genetic and epigenetic alterations (e.g., microRNAs), these pathobiological events ultimately lead to RV dilation and failure ("decompensated RVH") (Agrawal et al., 2020; van der Bruggen et al., 2017). Right ventricular hypertrophy may occur in the setting of RV outflow tract obstruction (PS; normal pulmonary vascular resistance) or in hypertensive pulmonary vascular disease with anatomically normal RV outflow (Hansmann, 2017; Hansmann et al., 2019; Santens et al., 2020). Both etiologies have been studied in various animal models (Andersen et al., 2020); however, none of them fully simulate *human* RVH *in vivo* (Agrawal et al., 2020; Andersen et al., 2020; Bernardo et al., 2020; Santens et al., 2020).

The hallmarks of maladaptive decompensated cardiac hypertrophy are cell death, fibrosis, dysregulation of Ca^{2+}-handling proteins, mitochondrial dysfunction, metabolic reprogramming, reactivation of fetal gene expression, altered sarcomere structure, and insufficient angiogenesis (Agrawal et al., 2020; Nakamura and Sadoshima, 2018). More specifically, a number of microRNAs (miRNAs) have been suggested to be involved in the pathobiology of RV hypertrophy and dysfunction in conditions of high pressure afterload (pulmonary hypertension or PS/pulmonary artery banding). However, the vast majority of such studies have been conducted on rodent heart tissues, postmortem human cardiac specimen, and/or circulating RNAs (see discussion and refs. Bittel et al., (2011); Bittel et al. (2014); Chouvarine et al., 2020; O'Brien et al. (2012); Wang et al. (2014); Yang et al. (2013); Zhang et al. (2013)), but not on freshly isolated human myocardium.

Since non-coding RNAs, especially long non-coding RNAs (lncRNAs) and circular RNAs (circRNAs), are not well conserved between species (e.g., mouse/rat versus human [Gandhi et al., 2019; Jakobi et al., 2020]), we chose an exploratory study design in two well-matched patient cohorts that are distinguished by the

[1]Department of Pediatric Cardiology and Critical Care, Hannover Medical School, Hannover, Germany

[2]Departments of Pediatric Cardiology and Pediatric Cardiac Surgery, German Heart Institute, German Center for Cardiovascular Research (DZHK) partner site Berlin, Berlin, Germany

[3]Departments of Pediatric Cardiology and Pediatric Cardiac Surgery, Friedrich-Alexander University of Erlangen-Nürnberg, Erlangen, Germany

[4]Divisions of Pediatric Cardiology and Pediatric Cardiac Surgery, Heart Center, University of Kiel, German Center for Cardiovascular Research (DZHK) partner site Hamburg/Kiel/Lübeck, Kiel, Germany

[5]Competence Network for Congenital Heart Defects (CNCHD), Berlin, Germany

[6]National Register for Congenital Heart Defects, German Center for Cardiovascular Research (DZHK), Berlin, Germany

[7]Lead contact

*Correspondence: georg.hansmann@gmail.com

https://doi.org/10.1016/j.isci.2021.102232

presence or absence of RVH due to RV outflow tract obstruction (TOF/PS versus ventricular septal defect without PS). TOF is a congenital heart disease with four anatomical features: (1) pulmonary artery stenosis, (2) ventricular septal defect (VSD), (3) deviation of the origin of the aorta (septal overriding aorta), and (4) concentric RVH.

We hypothesized that specific transcriptional programs exist in the human hypertrophied, non-failing RV of infants with TOF/PS versus the non-hypertrophied RV of infants without PS (VSD only), reflecting features of fetal gene programming and altered glucose/lipid metabolism. Comprehensive understanding of such transcriptional RNA profiles and networks requires quantification of competing endogenous RNA, which consists of a variety of non-coding RNAs and protein-coding RNAs competing as targets of miRNA regulation (Salmena et al., 2011).

To identify the transcriptional profiles characteristic of human RVH, we analyzed differentially expressed genes (DEGs) by sequencing messenger RNAs (mRNAs), long non-coding RNAs (lncRNAs), and circular RNAs (circRNAs) in human RV tissue. Additionally, shorter regulatory microRNAs (miRNA) were also sequenced. Analysis of potential regulatory networks based on target specificity of the differentially expressed miRNAs to the DEGs in this study allowed us to unravel key miRNAs likely involved in transcriptional adaptation in RVH with increased pressure afterload. Apparently, most relevant regulatory miRNAs are simultaneously epigenetically regulated by several circRNAs and lncRNAs, which sponge the miRNAs interacting with them, thereby reducing the regulatory capacity of these miRNAs. Moreover, using only sets of differentially expressed RNAs, we show that less biologically relevant miRNAs are regulated to a much lower degree by lncRNAs and circRNAs, compared with the most relevant regulatory miRNAs.

RESULTS

Demographics of the study cohort

The study included 19 infants with TOF/PS and eight controls with VSD without PS, 2–12 months old, undergoing surgical repair of the underlying congenital heart disease at three tertiary centers. Demographics data are summarized in Table 1, and individual information is provided in Table S1. The two groups were similar in terms of age and weight.

Cardiac mRNA expression in human RV hypertrophy has a specific profile dependent on sex and age

After subtraction of age- and sex-specific genes (see methods), a total of 500 DEGs (false discovery rate [FDR] <0.05) were detected, of which 141 were upregulated and 359 were downregulated. Additionally, we identified 23 DEGs specific to sex, i.e., differentially expressed between males and females in both TOF/PS and VSD groups, and 41 genes specific to age, i.e., differentially expressed between older (7–8 months) and younger (2–4 months) patients in both TOF/PS and VSD groups. Figure 1 shows a heatmap of differentially expressed genes with fold changes ≥ 2 or ≤ 0.5 identified by comparisons of the entire TOF/PS (labeled: TOF) and VSD cohorts; it also shows the corresponding fold changes and FDR-adjusted p values of the same genes in five additional comparisons stratified by sex and age. The differential expression profiles in males, and those in the younger subgroup (2–4 months old), generally were consistent with those of the entire cohort (Figure 1). Female-specific transcriptional regulation and the developmental changes in the older subgroup (7–8 months old) bring in additional regulatory signaling, making identification of the disease-related transcriptional regulation in these subgroups more challenging. The heatmap in Figure 1 represents the DEGs after removal of the sex- and age-specific genes (see methods for details). Many biological processes relevant to human adaptive (compensated) RVH in TOF/PS versus VSD controls are represented by the top DEGs shown in Figure 1, e.g., TGF-β regulation of extracellular matrix (SERPINA3, CEBPD, ELN, SERPINE1, LTBP2, AEBP1, IGF1, CTGF, SFRP4, ALDH1A3, UCHL1, CTSK, DDIT4, COL8A2, ID4, NRCAM, SCRG1, CFB); fibrosis regulation by small leucine-rich proteoglycan (BGN and FMOD); gap junction pathways for regulation of intercellular current flow (TUBA3E, TUBA3D, HTR2B, HTR2A); receptor for advanced glycation end (RAGE) pathway (SERPINE1, IGF1, CTGF); collagen biosynthesis (COL25A1, COL8A2, COL9A2); lipid metabolism (HMGCS2 and CTGF); etc. To identify the RVH pathways that are significantly overrepresented by DEGs in the entire cohort (with age- and sex-specific genes excluded) and the five age- and sex-stratified subgroups, we used the BioPlanet pathway annotation (the results are shown in Data S1). Several pathways were noticeably more overrepresented by the TOF/PS versus VSD DEGs in the females compared with the males. Most prominent examples of such pathways are the brain-derived neurotrophic factor (BDNF) signaling pathway (27 DEGs in females versus 15 DEGs in males) and the collagen biosynthesis and modifying enzymes pathway (15 DEGs in females versus 6 DEGs in males). Similarly, overrepresentation of pathways

Table 1. Characteristics of all patients with TOF/PS and VSD controls

Patients	VSD controls n = 8	TOF/PS n = 19	p value
Demographics			
Age (months)	6.1 ± 3.5	5.4 ± 1.3	n.s.
Older (7–8 months), n = 9	9.0 ± 2.2	7.2 ± 0.4	n.s.
Young (2–4 months), n = 8	2.7 ± 1.2	3.4 ± 0.5	n.s.
Between (5–6 months), n = 10	5	5.4 ± 0.5	n.s.
Count by age, n	8	19	
Older (7–8 months)	4	5	
Young (2–4 months)	3	5	
Between (5–6 months)	1	9	
Sex, female, n (%)	5 (63%)	7 (37%)	
Older (7–8 months)	3 (75%)	2 (40%)	
Young (2–4 months)	1 (33%)	2 (40%)	
Between (5–6 months)	1 (100%)	3 (33%)	
Body height, cm	62.6 ± 5.2	66.6 ± 4.4	n.s.
Older (7–8 months)	66.0 ± 3.6	68.5 ± 6.1	n.s.
Young (2–4 months)	60.3 ± 4.9	63.0 ± 4.2	n.s.
Between (5–6 months)	56	66.6 ± 2.8	n.s.
Body weight, kg	5.6 ± 1.5	6.9 ± 1.0	0.008
Older (7–8 months)	6.7 ± 1.2	7.8 ± 1.1	n.s.
Young (2–4 months)	4.6 ± 1.2	5.8 ± 0.2	n.s.
Between (5–6 months)	4.3	6.9 ± 0.9	n.s.
RVOTO (RV pressure afterload)			
RVOT CW Doppler, m/s	NA	4.7 ± 1.1	
Older (7–8 months)	NA	5.0 ± 1.5	
Young (2–4 months)	NA	4.7 ± 0.8	
Between (5–6 months)	NA	4.4 ± 1.1	
Oxygen saturation (SpO_2), %	99.3 ± 1.3	90.9 ± 8.6	0.0125
Older (7–8 months)	99.0 ± 1.7	91.6 ± 8.6	n.s.
Young (2–4 months)	99.3 ± 1.5	88.9 ± 10.4	n.s.
Between (5–6 months)	100	92.0 ± 9.1	n.s.

BSA, body surface area; CW, continuous wave; NA, non-applicable; n.s., not significant; RV, right ventricle; RVOT, RV outflow tract; RVOTO, RVOT obstruction; TOF, tetralogy of Fallot; VSD, ventricular septal defect.
For individual patient data, see also Table S1.
Values are presented as mean ± SD. A Wilcoxon signed-rank test was applied. $p < 0.05$ was considered significant.

was also age dependent. For example, the TGF-β regulation of extracellular matrix pathway had 42 DEGs in the younger group (2–4 months) versus 15 DEGs in the older group (7–8 months). Analysis of the Gene Ontology (GO) biological process terms overrepresented by DEGs among the subgroups showed that age and sex have significant effects on the RVH-associated gene expression profile (Figure S1). To visualize the significance of the age and sex effects, compared with the RVH effect, on the overall gene expression, we performed principal-component clustering analysis that revealed all three effects as appreciable and also showed absence of outliers (Figure S2).

miRNA expression analysis reveals potential epigenetic regulators of human RVH

To investigate gene expression regulation in RVH by miRNAs, we performed separate sequencing of mature miRNAs, which are single-stranded RNA molecules approximately 21–23 nucleotides long (Farazi et al., 2008), i.e., shorter than the other RNAs sequenced in this study (>200 nt). Differentially expressed miRNAs with fold changes and p values are presented in Table S2. The following miRNAs were significantly (FDR<0.05)

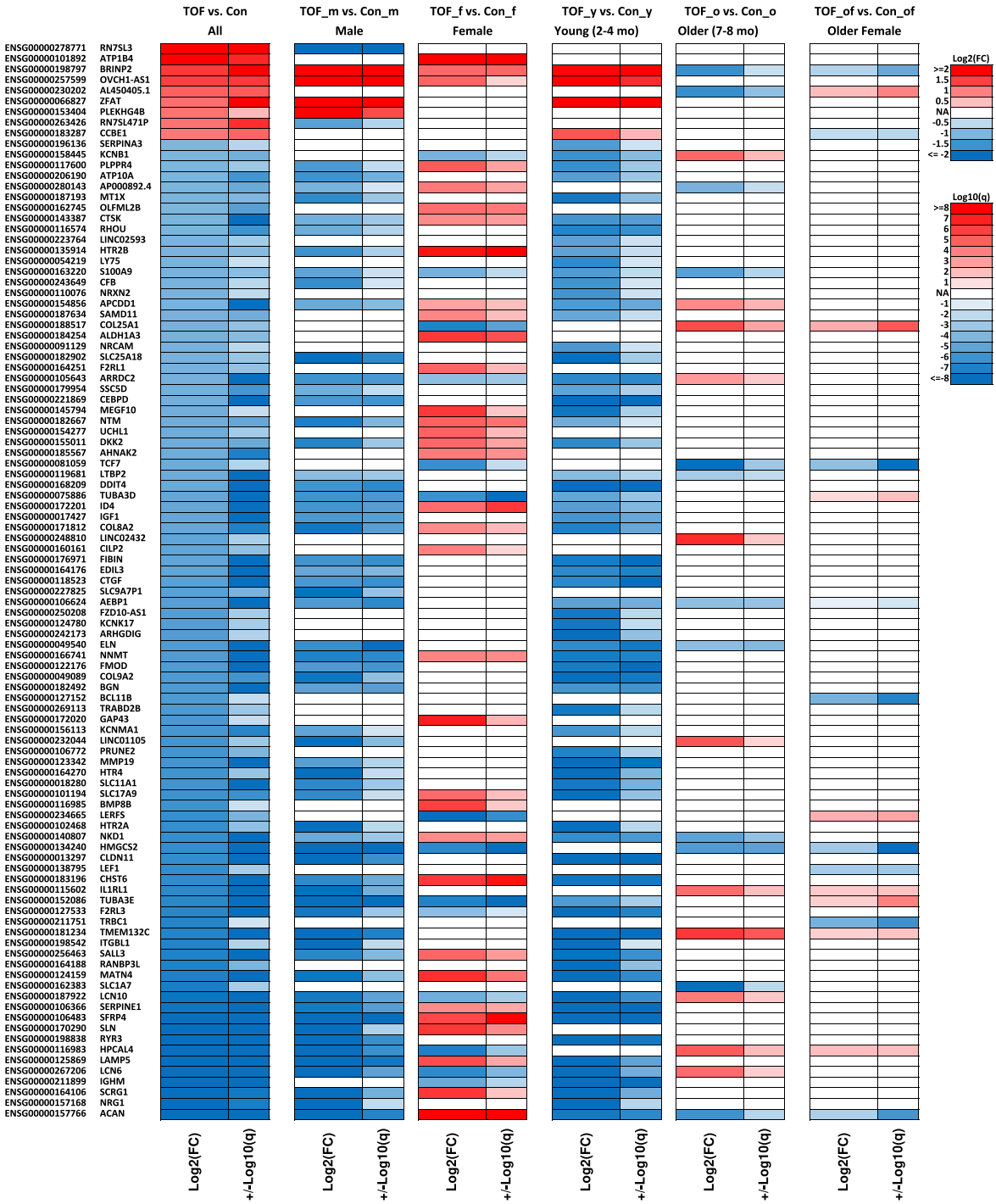

Figure 1. Heatmap of differentially expressed genes shows more consistent expression profiles in male and young groups and more diverse gene expression in female and older groups

The heatmap shows 101 genes that were significantly differentially expressed (FDR<0.05) and had fold change <0.5 or >2 in the All group (based on all samples in the study), from which the age- and sex-specific genes were excluded. The age-specific genes were defined as found in both TOF_old versus TOF_young and Con_old versus Con_young comparisons. The sex-specific genes were defined as found in both TOF_m versus TOF_f and Con_m versus Con_f comparisons. The five comparisons, shown in the heatmap after the All group comparison, contain only those differentially expressed genes (regardless of the fold change) that correspond to the selection of genes in the All group. The group sizes are as follows: All: N_{TOF} = 19, N_{Con} = 8; Male: N_{TOF} = 12, N_{Con} = 3; Female: N_{TOF} = 7, N_{Con} = 5; Young: N_{TOF} = 5, N_{Con} = 3; Older: N_{TOF} = 5, N_{Con} = 4; Older female: N_{TOF} = 2, N_{Con} = 3.

differentially expressed (1) in the entire cohort: miR-31↑, miR-33b↓, miR-135a-2↓, miR-188↓, miR-216a↓, miR-323b↓, miR-371a↑, and miR-372↑; (2) in males: miR-31↑ and miR-217↓; (3) in females: miR-372↑; (4) in the young group (2–4 months): none; (5) in the older group (7–8 months): miR-184↓, miR-216a↓, miR-4423↓, miR-4999↓, and miR-5008↓; and (6) in older females: miR-33a↓, miR-216a↓, miR219a-1↓, and miR-5008↓ (the arrows show the direction of regulation). Of note, miR-31, miR-216a, miR-372, and miR-5008 co-occur in the overall cohort and several age/sex subgroups, each with the same direction of regulation; thus these four miRNAs are likely involved in strong epigenetic regulation occurring in RVH in TOF/PS. On the other hand, based on their membership in the aforementioned subgroups, these four miRNAs can be associated with RVH in certain subgroups: in males: miR-31; in females: miR-372; and in older patients: miR-216a and miR-5008.

Differential expression of sponging circRNAs and lncRNAs indicates age- and sex-specific regulation of non-coding RNAs in high pressure load conditions such as TOF/PS (RVH)

To be able to construct regulatory networks of non-coding RNAs, we conducted differential expression analysis of circRNAs and lncRNAs. lncRNAs and circRNAs are capable of sponging miRNAs, thereby reducing their availability to act as inhibitors of both sustained expression of mRNA and further translation of functional peptides/proteins. Differentially expressed circRNA isoforms and lncRNAs with fold changes and p values are reported in Tables S3 and S4, respectively. Interestingly, except for lncRNAs PAX8-AS1 and AC083843.3, the sponging molecules (lncRNAs or circRNAs) are not co-occurring in the age- or sex-stratified subgroups, suggesting age- and sex-specific non-coding RNA regulation in high pressure load conditions such as TOF/PS, via transcriptional regulation by circRNAs and lncRNAs (see Tables S3 and S4 for differential expression of circRNAs and lncRNAs in the overall cohort and subgroups).

mRNA-miRNA-circRNA/lncRNA interaction networks reflect differences in age- and sex-specific epigenetic RVH regulation

Combining the expression data with the miRNA gene target information (miRDB, TargetScan) and the circRNA/lncRNA target information obtained by the TargetScan algorithm (see methods), we were able to create a network of transcriptional regulation in the hypertrophied myocardium undergoing adaptation to high RV pressure load (Figures 2 and 3). Figure 2 shows the major regulatory effects of the differentially expressed miRNAs and their differentially expressed epigenetic regulators (circRNA and lncRNA sponges) on the genes known to mediate cardiac hypertrophy, fibrosis, cardiac dysfunction/decreased contractility, and other associated pathobiological events. We show some of these key genes if they were differentially expressed in our datasets (e.g., SIK1, FABP4, PIK3IP1), or could be tentatively called up- or downregulated based on their fold change, i.e., $|\mathrm{Log}_2(\text{Fold Change})| \geq 0.14$ (target genes in Figure 2A and genes shown in green in Figure 2B). Importantly, we observed that miRNAs with most biologically relevant key gene targets (mRNA transcripts) are also sponged by the highest number of non-coding RNAs, which reveals the significance of this level of epigenetic regulation: As evident from Figure 2A, miRNAs not targeting any known key genes are practically not regulated by lncRNAs or circRNAs. Additionally, we created regulatory networks showing DEGs (mRNA) regulated by the differentially expressed miRNAs in both the entire cohort (Figure 3A) and in older females (Figure 3B). Although the target genes in Figure 3 consist of a large number of less known genes associated with cardiac hypertrophy, their functional annotation shows strong involvement in the biological processes potentially associated with RVH (e.g., TGF-β regulation of ECM, focal adhesion, etc.). Additionally, we created the same type of interaction networks for female-, male-, and older subgroups (Figure S3). The "younger" group (2–4 months old) was not evaluated further, because no differentially expressed miRNAs were identified for this group.

Differentially expressed lncRNAs have predicted DNA/mRNA/protein interactions, whereas no predicted interactions (circRNA-mRNA/protein) were found for the differentially expressed circRNAs

Non-coding RNA, such as lncRNAs, can affect (either promote or suppress) gene expression in *cis* (i.e., near the loci from which these lncRNAs are transcribed) via a variety of mechanisms (Gil and Ulitsky, 2020). Moreover, lncRNAs and circRNAs can directly interact with mRNAs (affecting their pre-mRNA splicing, RNA editing, mRNA stability control, translation activation, or prevention of miRNA-induced repression) (Szczesniak and Makalowska, 2016) and proteins (Lin et al., 2020). lncRNA/circRNA- miRNA interactions are the most straightforward to interpret, due to the expected transcript degradation or translational inhibition effect of miRNAs on their targets. However, for completeness, we also checked whether cataloged lncRNA-DNA/mRNA/protein

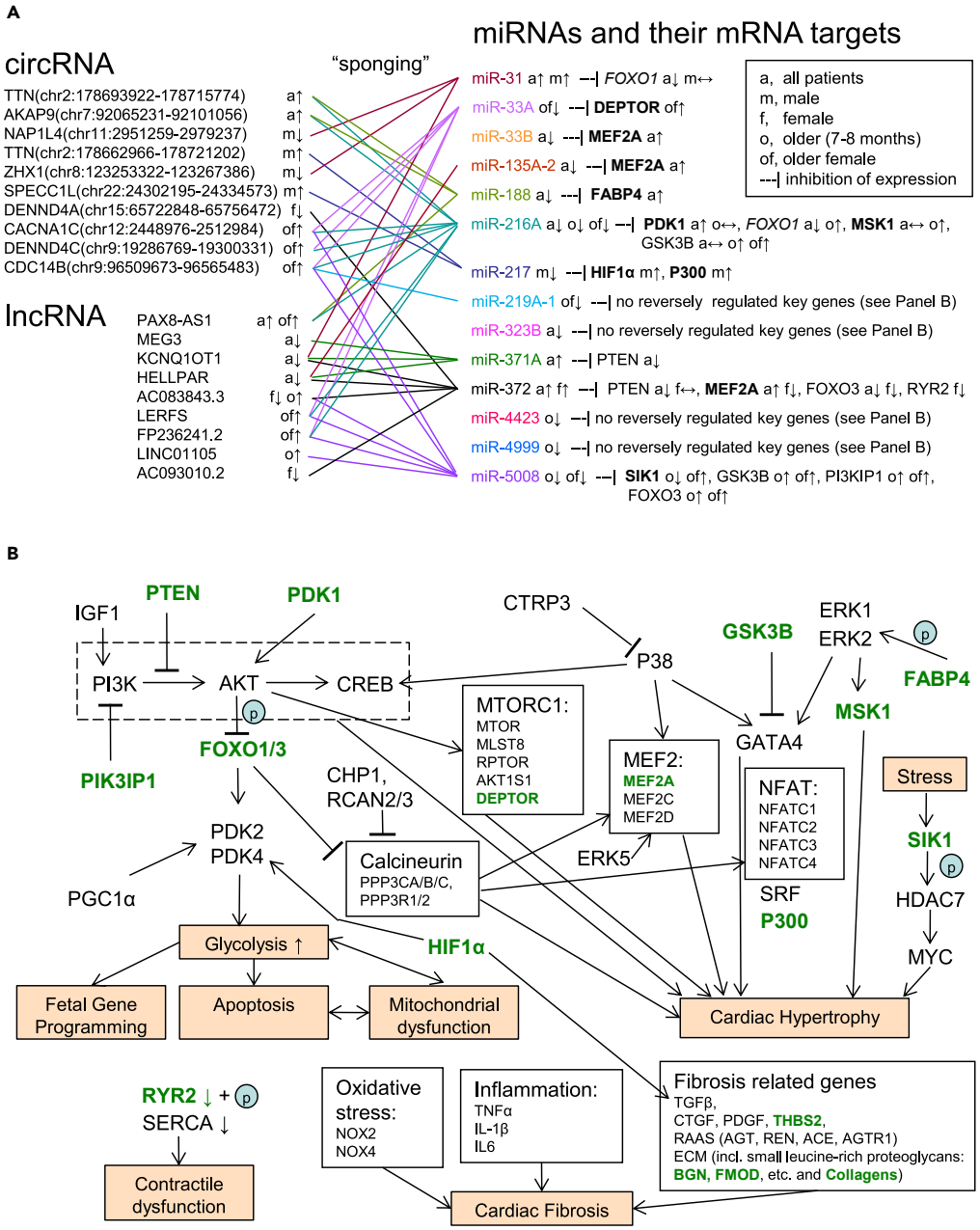

Figure 2. Epigenetic regulation of key genes involved in processes associated with cardiac hypertrophy by miRNA silencing of gene expression and the sponging effects of circular RNA and long non-coding RNA

Here, we only show predicted circRNA-miRNA-mRNA and lncRNA-miRNA-mRNA interactions, in which regulation changes direction, e.g., upregulated circRNA-downregulated miRNA-upregulated mRNA, thus suggesting involvement of the miRNA and the corresponding sponging non-coding RNA in the regulation of gene expression. The regulation direction is based on various TOF/PS versus Control comparisons (a = all patients with TOF/PS and VSD controls; m = male TOF/PS and VSD; f = female TOF/PS and VSD; o = older, i.e., 7–8 months old, TOF/PS and VSD; of = older female TOF/PS and VSD). The direction of regulation is indicated by the arrows: ↑ upregulation, ↓ downregulation, ↔ no change ($|Log2(Fold\ Change)| < 0.14$, i.e., $0.9 > Fold\ Change < 1.1$). All differentially expressed miRNAs are included in (A). Genes shown in (A) are in bold font if their expression is known to positively correlate with the effects of cardiac hypertrophy. Genes shown in italics have a double role and may be both pro- and anti-hypertrophic. Genes shown in green font in (B) are likely modulated by the circRNA/lncRNA-miRNA epigenetic control (based on our findings) as shown in (A). With the exception of miR-33B, miRNAs regulated by multiple sponging circRNA/lncRNA appear to exert more epigenetic regulation on key genes associated with cardiac hypertrophy, i.e., it appears that all available modes of epigenetic regulation are employed for quick transition to the hypertrophic cardiomyocyte state.

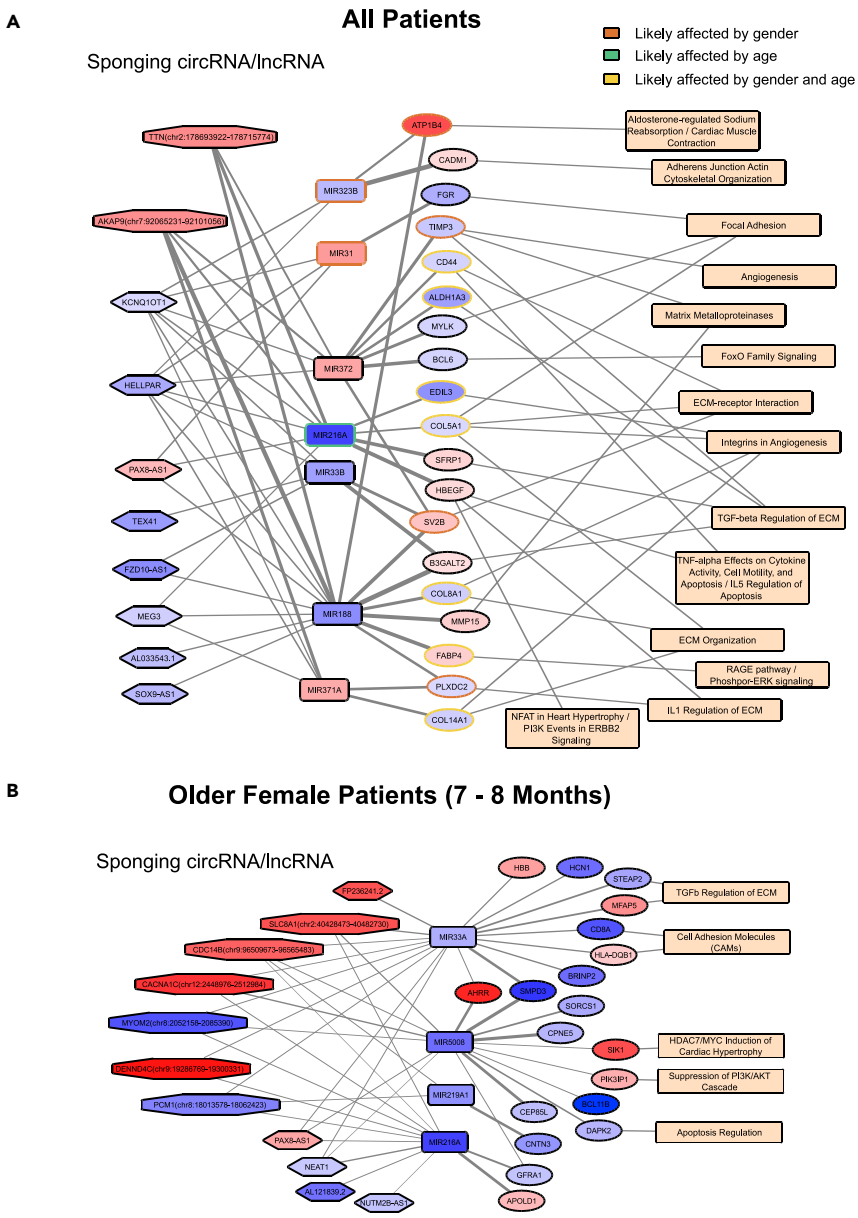

Figure 3. Competing endogenous RNA regulates DEGs and their functions associated with cardiac hypertrophy

(A) Epigenetic regulation network based on the predicted interactions among differentially expressed molecules of the All group (based on all samples in the study [N_{TOF} = 19, N_{Con} = 8]), from which the age- and sex-specific genes were excluded. The age-specific genes were defined as found in both TOF_old versus TOF_young and Con_old versus. Con_young comparisons. The sex-specific genes were defined as found in both TOF_m versus TOF_f and Con_m versus Con_f comparisons. For space considerations only DEGs with relevant functions are presented. Genes shown with brown border may be affected by sex (were also found in TOF_m versus Con_m and/or TOF_f versus Con_f). Genes shown with green border may be affected by age (were also found in TOF_old versus Con_old and/or TOF_young versus Con_young). Genes shown with yellow border may be affected by both sex and age.

(B) The same type of an interaction network is shown for the older female group (N_{TOF} = 2, N_{Con} = 3). Nodes are colored blue if downregulated, and red if upregulated. LncRNAs are shown as hexagons, circRNAs are shown as octagons. Line thickness represents the miRNA target score (see methods). Functional annotation was obtained primarily from the NCATS BioPlanet (https://tripod.nih.gov/bioplanet/).

interactions and circRNA-mRNA/protein interactions from the RNA Interactome database (RNAInter) (Lin et al., 2020) exist for the differentially expressed RNA in our study. We did not find such interactions with the circRNAs, but we found cataloged lncRNA-DNA/mRNA/protein interactions (see Data S2).

Co-expression networks in RVH (TOF/PS) compared with those in controls (VSD) identify gene clusters of RVH adaptation to high pressure load

To elucidate which of the overrepresented pathways (based on the proportion of DEGs) are truly involved in the biological processes specific to the corresponding phenotype of compensated RVH, we employed co-expression analysis; by doing so, we narrowed the list of these pathways based on the co-expression profiles of the participating genes. We performed co-expression analysis using the partial correlation coefficient with information theory (PCIT) approach (see methods for details). Subsequently we unraveled one VSD control co-expression cluster (with KCNMA1 as the "hub") and four TOF/PS RVH clusters (with THBS3, FKBP10, BGN, and SALL3 as the "hubs"). Such gene clusters likely represent a biological process driven by directly or indirectly interacting molecules. Moreover, these clusters can be specific to a condition, e.g., TOF/PS, and span multiple pathways, thereby providing an additional level of functional relation annotation among the identified DEGs. Table S5 lists the pathways overrepresented by the DEGs from these five clusters. The pathways of the TOF/PS clusters largely recapitulate the findings of the differential expression analysis (see Data S1 and Table S5 for comparison). Additional pathways identified using this method included: (1) small leucine-rich proteoglycan (SLRP) molecules (BGN and FMOD); (2) cell adhesion molecules (CAMs; CLDN11, VCAN, NLGN2, ITGA8, NRXN2, NRCAM); (3) keratan sulfate/keratin metabolism (ACAN, CHST6, FMOD, CHST2); and (4) inflammatory response (COL1A2, FN1, THBS3).

Multiple molecules (mRNA) from the same co-expression cluster are likely targets of a single regulatory RNA (miRNA or lncRNA). Therefore, we also checked whether some differentially expressed miRNAs and lncRNAs target mRNA and/or DNA of multiple DEGs in each of the co-expression clusters. Interestingly, miR-371a, miR-372, and to a lesser degree miR-33 (all upregulated) likely downregulate several genes in the co-expression clusters (Table S5). lncRNAs BANCR and HELLPAR interact with a few mRNAs in the co-expression clusters (Table S5). lncRNAs MEG3 and RMRP have a large number of DNA interactions with DEGs of the co-expression clusters (Table S6).

DISCUSSION

We conducted the first study of human RV cardiac hypertrophy by means of comprehensive RNA expression and RNA interaction network analysis, including predicted sponging of miRNA by circRNA and lncRNA. Previous human RVH RNA expression studies relied on postmortem control tissue to study mRNA expression (Bittel et al., 2011; O'Brien et al., 2012; Wang et al., 2014; Yang et al., 2013), expression of miRNA (Zhang et al., 2013), and expression of miRNA and small no-non coding RNA (Bittel et al., 2014; O'Brien et al., 2012; Wang et al., 2014). Therefore, the results of these studies on postmortem tissue cannot be used for direct comparison with our data that is based on intraoperatively harvested, freshly snap frozen RV tissue. Moreover, all the previous studies used microarray panels, further complicating possible comparison with our RNA sequencing results.

On the mRNA level, we report DEGs overrepresented in pathways that have been reported to be involved in cardiac hypertrophy, as further discussed in the supplemental information. Another important finding in our current study on compensated RVH (compensated RVH in TOF/PS; in the "All" group), is the possibly compensatory upregulation of FABP4, a fatty acid-binding protein known to positively regulate cardiac hypertrophy via activation of the ERK signaling pathway (Zhang et al., 2016). Consistently, we had previously demonstrated FABP4 downregulation in the RV of patients with end-stage PH with decompensated RVH and heart failure (Legchenko et al., 2018). We had also shown that the PPARγ agonist pioglitazone induces RV and cardiomyocyte FABP4 mRNA expression (Legchenko et al., 2018) that was associated with reversal of both RV dysfunction and severe PH in rats exposed to VEGFR2 blockade (SU5416) and hypoxia (Legchenko et al., 2018).

On the non-coding RNA level, we report for the first time miRNAs, lncRNAs, and circRNAs associated with human RVH (Tables S2–S4). To our knowledge, previous reports identified several miRNAs associated with either LVH in high pressure afterload models (Mohan et al., 2018; Rau et al., 2017; Wehbe et al., 2019), RVH in rodent pulmonary artery (PA) banding models (Andersen et al., 2020; Reddy and Bernstein, 2015; Reddy et al., 2012; Thum and Batkai, 2014), or human RVH with postmortem control samples (Bittel et al., 2014; O'Brien et al., 2012; Wang et al., 2014; Zhang et al., 2013). We did not find any of the miRNAs previously reported in cardiac

hypertrophy of animals or humans, with the exception of miR-216a and miR-217, which were downregulated in human compensated RVH in our study (see the supplemental information for extended discussion).

lncRNAs are RNA molecules that can modulate gene expression via several mechanisms: signaling induced by transcription factors, miRNA sponging, recruiting chromatin-modifying enzymes, and molecular scaffolding resulting in histone modification (Wang and Chang, 2011). Within the scope of our study, we concentrated on the decoy function (miRNA sponging) of lncRNAs. Reportedly, Mhrt, Chast, CHRF, ROR, H19, Plscr4, and MIAT are associated with cardiac hypertrophy, and MALAT1, wisper, MEG3, and H19 are involved in ECM remodeling (reviewed in Zhou et al., 2019, and Liu and Tang, 2019). Additionally, Uca1 (Zhou et al., 2018) and Peg10 (Wen et al., 2019) have been reported as modulators of LVH via Hoxa9 in mouse TAC models, whereas Kcnq1ot1 was shown to sequester miR-30e-5p to release Adam9 thereby inducing cardiac hypertrophy in angiotensin II-stimulated hypertrophic cardiomyocyte cell culture (Wang et al., 2020). From the aforementioned list of lncRNAs compiled from the published literature on LVH, we found MEG3 and KCNQ1OT1 to be significantly downregulated in human compensated RVH in our study (further discussed in the supplemental information). Interestingly, a recent study used quantitative PCR of RV endomyocardial biopsies taken from patients with end-stage PH and postmortem or aortic valve stenosis controls, to show that the lncRNA H19 is upregulated in decompensated RVH (Omura et al., 2020). In RV pressure overload models (monocrotaline, PA banding), lncRNA H19 expression progressively increased (from the compensated to decompensated state), becoming upregulated in the decompensated but not in the compensated RV of rats with pressure overload (Omura et al., 2020). Our study subjects (infants with TOF/PS) had adaptive, compensated RVH without RV dilation and failure: The lncRNA H19 was slightly upregulated (fold change 1.17), but not differentially expressed (q-value 0.56) in the overall cohort. Thus, we speculate that lncRNA H19 in humans is progressively upregulated in the hypertrophied RV as it transitions from preserved volume and function, to dilation and heart failure.

To our knowledge, at present there are no published circRNA studies on human RVH. Comparison of our current results with published mouse LVH models is discussed in the supplemental information.

In our circ/lncRNA-miRNA-mRNA interaction network (Figure 2A), RVH-associated miRNAs targeting key cardiac hypertrophy genes appear to have the most sponging circ/lncRNA regulators/decoys. Clearly regulated key genes (Figure 2A) include PTEN, downregulated by combined action of miR-372 (with five ncRNA decoys) and miR-371A (with three ncRNA decoys); PDK1 and MSK1, upregulated by miR-216A (with eight ncRNA decoys); and GSK3B, PI3KP1, and FOXO3, upregulated by miR-5008 (with six ncRNA decoys). Such heavy reliance on epigenetic regulation indicates that the known pro-hypertrophic pathways enabled by these genes (PTEN, PDK1, GSK3B [Dorn and Force, 2005]; MSK1 [Markou et al., 2009]; PI3KIP1 [Song et al., 2015]; and FOXO3 [Ni et al., 2006]) are particularly important in human compensated RVH.

Gene co-expression analysis gave us another way to gain insight into key biological processes in human compensated RVH. An extended discussion on the uncovered pathways using this method is provided in the supplemental information. Interestingly, the miRNAs miR-371a and miR-372, described earlier, are also predicted to target multiple differentially expressed, RVH-related genes in the co-expression modules (Table S5). This discovery underlines the significance of these miRNAs (miR-371a and miR-372) as potential biomarkers and/or therapeutic targets for diseases associated with RV pressure load.

The strength of our study is the first comprehensive view of transcriptomic expression in human RVH *in vivo*. To the best of our knowledge, ours is the first study exploring lncRNA and circRNA expression, as well as miRNAs, in human RVH. This is particularly important because lncRNA and circRNA have poor species conservation, so that cell culture and animal studies are difficult to translate to human diseases.

Limitations of the study

Our study also has certain limitations. Owing to the large volume of data, the regulatory mechanisms that we present are based largely on *in silico* predictions—their validation will need to be conducted in subsequent research. The reported regulatory network presented in Figure 2A was not validated by qPCR of cDNA derived from cardiac tissue or cardiomyocyte cell culture studies. Thus we cannot completely ascertain to which degree the presented miRNAs are involved in regulation of the target genes and whether or not other mechanisms may also play a role in regulation of the key genes shown. Because cardiac surgery on the patients with TOF/PS (compensated RVH) and VSD (control) had to be performed within the first year

of life, our findings may not fully reflect RVH in older patients. However, we did exclude neonates (first postnatal month) as they undergo postnatal adaption of pressure and flow in their circulation, and performed subgroup analyses by age and sex. Finding non-surgical human, freshly isolated RVH and non-RVH samples for a representative *in vivo* study is difficult (ethics, consent), but has been pursued in adults with scleroderma-associated or idiopathic PH, via RV septal endomyocardial biopsies (Hsu et al., 2018). Recently, a specific RNA signature of tissue fibrosis and enrichment of beneficial metabolic regulators (AMPK, PPARs) was identified in animal models of organ fibrosis, i.e., kidney, liver, and lung (Zhang et al., 2020) and the failing RV in severe PH (Legchenko et al., 2018). Of note, it has been postulated that mild to moderate fibrosis prevents dilation (cardiomyocyte overstretch) of the hypertrophied ventricles (Andersen et al., 2019). In contrast, we found only a moderate induction of a pro-fibrosis mRNA expression signature in the hypertrophied RV of patients with TOF/PS (downregulation of BGN and FMOD), probably because of the high adaptivity and plasticity of the infant myocardium, and the rather short duration of high pressure afterload.

Taken together, we provide comprehensive RNA expression profiles, signaling characteristics, and network analysis of human RVH due to high pressure afterload (compensated RVH, no RV failure). The miRNAs reported here are at the core of this transcriptomic regulation in compensated (adaptive) RVH and, as such, are potential targets of heart failure therapies and/or biomarkers of disease severity/progression. Validation of the predicted competing endogenous RNA interactions (sponging of miRNA by circRNA and lncRNA) and further investigation of the regulatory mechanisms should be a focus of future research.

Resource availability

Lead contact

Georg Hansmann, Department of Pediatric Cardiology and Critical Care, Hannover Medical School, Carl-Neuberg-Str. 1, 30625 Hannover, Germany. E-mail: georg.hansmann@gmail.com.

Materials availability

Further information and requests for resources and reagents should be directed to and will be fulfilled by the lead contact, Georg Hansmann (georg.hansmann@gmail.com), according to the material transfer agreement (MTA). This study did not generate new unique reagents.

Data and code availability

This study did not generate any software, except for Perl/bash scripts for subtracting circRNA read counts from the total RNA read count data, which are deposited to https://github.com/pch-code/circ-scripts. Sequencing data are not publicly available due to consent restrictions. Upon request, the data can be made available via controlled access (National Register for Congenital Heart Defects, Berlin, Germany).

METHODS

All methods can be found in the accompanying transparent methods supplemental file.

SUPPLEMENTAL INFORMATION

Supplemental information can be found online at https://doi.org/10.1016/j.isci.2021.102232.

ACKNOWLEDGMENTS

This study was supported by the German Research Foundation (DFG; HA4348/6-2 KFO311 to G.H.). Dr. Hansmann receives additional funding from the German Research Foundation (DFG; HA4348/2-2), the Federal Ministry of Education and Research (BMBF ViP + program 03VP08053; BMBF 01KC2001B), and the European Pediatric Pulmonary Vascular Disease Network (www.pvdnetwork.org). The Competence Network for Congenital Heart Defects and the National Register for Congenital Heart Defects have received funding from the Federal Ministry of Education and Research, grant number 01GI0601 (until 2014), and the DZHK (German Center for Cardiovascular Research; as of 2015).

AUTHOR CONTRIBUTIONS

P.C. performed the data analysis and wrote the manuscript. J.P., R.C., J.S., U.M.M.B., T.P., H-H.K., S.D., and F.B. contributed to the acquisition of tissue samples and clinical data. G.H. generated the hypotheses,

developed the experimental design and concept of the study, performed RNA extraction and bioanalysis, obtained funding, and wrote the manuscript. All authors critically read and approved the manuscript.

DECLARATION OF INTERESTS

The authors declare no competing interests.

Received: November 9, 2020
Revised: January 28, 2021
Accepted: February 22, 2021
Published: March 19, 2021

REFERENCES

Agrawal, V., Lahm, T., Hansmann, G., and Hemnes, A.R. (2020). Molecular mechanisms of right ventricular dysfunction in pulmonary arterial hypertension: focus on the coronary vasculature, sex hormones, and glucose/lipid metabolism. Cardiovasc. Diagn. Ther. *10*, 1522–1540.

Andersen, A., van der Feen, D.E., Andersen, S., Schultz, J.G., Hansmann, G., and Bogaard, H.J. (2020). Animal models of right heart failure. Cardiovasc. Diagn. Ther. *10*, 1561–1579.

Andersen, S., Nielsen-Kudsk, J.E., Vonk Noordegraaf, A., and de Man, F.S. (2019). Right ventricular fibrosis. Circulation *139*, 269–285.

Bernardo, R.J., Haddad, F., Couture, E.J., Hansmann, G., de Jesus Perez, V.A., Denault, A.Y., de Man, F.S., and Amsallem, M. (2020). Mechanics of right ventricular dysfunction in pulmonary arterial hypertension and heart failure with preserved ejection fraction. Cardiovasc. Diagn. Ther. *10*, 1580–1603.

Bittel, D.C., Butler, M.G., Kibiryeva, N., Marshall, J.A., Chen, J., Lofland, G.K., and O'Brien, J.E., Jr. (2011). Gene expression in cardiac tissues from infants with idiopathic conotruncal defects. BMC Med. Genomics *4*, 1.

Bittel, D.C., Kibiryeva, N., Marshall, J.A., and O'Brien, J.E. (2014). MicroRNA-421 dysregulation is associated with tetralogy of fallot. Cells *3*, 713–723.

Chouvarine, P., Geldner, J., Giagnorio, R., Legchenko, E., Bertram, H., and Hansmann, G. (2020). Trans-right-ventricle and transpulmonary microRNA gradients in human pulmonary arterial hypertension. Pediatr. Crit. Care Med. *21*, 340–349.

Dorn, G.W., 2nd, and Force, T. (2005). Protein kinase cascades in the regulation of cardiac hypertrophy. J. Clin. Invest. *115*, 527–537.

Farazi, T.A., Juranek, S.A., and Tuschl, T. (2008). The growing catalog of small RNAs and their association with distinct Argonaute/Piwi family members. Development *135*, 1201–1214.

Gandhi, S., Ruehle, F., and Stoll, M. (2019). Evolutionary patterns of non-coding rna in cardiovascular biology. Noncoding RNA *5* (1), 15.

Gil, N., and Ulitsky, I. (2020). Regulation of gene expression by cis-acting long non-coding RNAs. Nat. Rev. Genet. *21*, 102–117.

Hansmann, G. (2017). Pulmonary hypertension in infants, children, and young adults. J. Am. Coll. Cardiol. *69*, 2551–2569.

Hansmann, G., Koestenberger, M., Alastalo, T.P., Apitz, C., Austin, E.D., Bonnet, D., Budts, W., D'Alto, M., Gatzoulis, M.A., Hasan, B.S., et al. (2019). 2019 updated consensus statement on the diagnosis and treatment of pediatric pulmonary hypertension: the European Pediatric Pulmonary Vascular Disease Network (EPPVDN), endorsed by AEPC, ESPR and ISHLT. J. Heart Lung Transplant *38*, 879–901.

Hsu, S., Kokkonen-Simon, K.M., Kirk, J.A., Kolb, T.M., Damico, R.L., Mathai, S.C., Mukherjee, M., Shah, A.A., Wigley, F.M., Margulies, K.B., et al. (2018). Right ventricular myofilament functional differences in humans with systemic sclerosis-associated versus idiopathic pulmonary arterial hypertension. Circulation *137*, 2360–2370.

Jakobi, T., Siede, D., Eschenbach, J., Heumuller, A.W., Busch, M., Nietsch, R., Meder, B., Most, P., Dimmeler, S., Backs, J., et al. (2020). Deep Characterization of circular RNAs from human cardiovascular cell models and cardiac tissue. Cells *9* (7), 1616.

Legchenko, E., Chouvarine, P., Borchert, P., Fernandez-Gonzalez, A., Snay, E., Meier, M., Maegel, L., Mitsialis, S.A., Rog-Zielinska, E.A., Kourembanas, S., et al. (2018). PPARgamma agonist pioglitazone reverses pulmonary hypertension and prevents right heart failure via fatty acid oxidation. Sci. Transl. Med. *10*, eaao0303.

Lin, Y., Liu, T., Cui, T., Wang, Z., Zhang, Y., Tan, P., Huang, Y., Yu, J., and Wang, D. (2020). RNAInter in 2020: RNA interactome repository with increased coverage and annotation. Nucleic Acids Res. *48*, D189–D197.

Liu, C.F., and Tang, W.H.W. (2019). Epigenetics in cardiac hypertrophy and heart failure. JACC Basic Transl. Sci. *4*, 976–993.

Markou, T., Cieslak, D., Gaitanaki, C., and Lazou, A. (2009). Differential roles of MAPKs and MSK1 signalling pathways in the regulation of c-Jun during phenylephrine-induced cardiac myocyte hypertrophy. Mol. Cell Biochem. *322*, 103–112.

Mohan, N., Kumar, V., Kandala, D.T., Kartha, C.C., and Laishram, R.S. (2018). A splicing-Independent function of RBM10 controls specific 3′ UTR processing to regulate cardiac hypertrophy. Cell Rep. *24*, 3539–3553.

Nakamura, M., and Sadoshima, J. (2018). Mechanisms of physiological and pathological cardiac hypertrophy. Nat. Rev. Cardiol. *15*, 387–407.

Ni, Y.G., Berenji, K., Wang, N., Oh, M., Sachan, N., Dey, A., Cheng, J., Lu, G., Morris, D.J., Castrillon, D.H., et al. (2006). Foxo transcription factors blunt cardiac hypertrophy by inhibiting calcineurin signaling. Circulation *114*, 1159–1168.

O'Brien, J.E., Kibiryeva, N., Zhou, X.G., Marshall, J.A., Lofland, G.K., Artman, M., Chen, J., and Bittel, D.C. (2012). Noncoding RNA expression in myocardium from infants with tetralogy of fallot. Circ. Cardiovasc. Genet. *5*, 279–286.

Omura, J., Habbout, K., Shimauchi, T., Wu, W.H., Breuils-Bonnet, S., Tremblay, E., Martineau, S., Nadeau, V., Gagnon, K., Mazoyer, F., et al. (2020). Identification of long noncoding RNA H19 as a new biomarker and therapeutic target in right ventricular failure in pulmonary arterial hypertension. Circulation *142*, 1464–1484.

Rau, C.D., Romay, M.C., Tuteryan, M., Wang, J.J., Santolini, M., Ren, S., Karma, A., Weiss, J.N., Wang, Y., and Lusis, A.J. (2017). Systems genetics approach identifies gene pathways and Adamts2 as drivers of isoproterenol-induced cardiac hypertrophy and cardiomyopathy in mice. Cell Syst. *4*, 121–128.e4.

Reddy, S., and Bernstein, D. (2015). Molecular mechanisms of right ventricular failure. Circulation *132*, 1734–1742.

Reddy, S., Zhao, M., Hu, D.Q., Fajardo, G., Hu, S., Ghosh, Z., Rajagopalan, V., Wu, J.C., and Bernstein, D. (2012). Dynamic microRNA expression during the transition from right ventricular hypertrophy to failure. Physiol. Genomics *44*, 562–575.

Salmena, L., Poliseno, L., Tay, Y., Kats, L., and Pandolfi, P.P. (2011). A ceRNA hypothesis: the Rosetta Stone of a hidden RNA language? Cell *146*, 353–358.

Santens, B., Van De Bruaene, A., De Meester, P., D'Alto, M., Reddy, S., Bernstein, D., Koestenberger, M., Hansmann, G., and Budts, W. (2020). Diagnosis and treatment of right ventricular dysfunction in congenital heart disease. Cardiovasc. Diagn. Ther. *10*, 1625–1645.

Song, H.K., Kim, J., Lee, J.S., Nho, K.J., Jeong, H.C., Kim, J., Ahn, Y., Park, W.J., and Kim, D.H. (2015). Pik3ip1 modulates cardiac hypertrophy by inhibiting PI3K pathway. PLoS One *10*, e0122251.

Szczesniak, M.W., and Makalowska, I. (2016). lncRNA-RNA interactions across the human transcriptome. PLoS One *11*, e0150353.

Thum, T., and Batkai, S. (2014). MicroRNAs in right ventricular (dys)function (2013 Grover Conference series). Pulm. Circ. *4*, 185–190.

van der Bruggen, C.E.E., Tedford, R.J., Handoko, M.L., van der Velden, J., and de Man, F.S. (2017). RV pressure overload: from hypertrophy to failure. Cardiovasc. Res. *113*, 1423–1432.

Wang, K.C., and Chang, H.Y. (2011). Molecular mechanisms of long noncoding RNAs. Mol. Cell *43*, 904–914.

Wang, W., Wu, C., Ren, L., Bao, Y., Han, Y., Li, C., and Li, Y. (2020). MiR-30e-5p is sponged by Kcnq1ot1 and represses Angiotensin II-induced hypertrophic phenotypes in cardiomyocytes by targeting ADAM9. Exp. Cell Res. *394*, 112140.

Wang, X.M., Zhang, K., Li, Y., Shi, K., Liu, Y.L., Yang, Y.F., Fang, Y., and Mao, M. (2014). Screening miRNA and their target genes related to tetralogy of Fallot with microarray. Cardiol. Young *24*, 442–446.

Wehbe, N., Nasser, S.A., Pintus, G., Badran, A., Eid, A.H., and Baydoun, E. (2019). MicroRNAs in cardiac hypertrophy. Int. J. Mol. Sci. *20* (19), 4714.

Wen, Z.Q., Li, S.H., Shui, X., Tang, L.L., Zheng, J.R., and Chen, L. (2019). LncRNA PEG10 aggravates cardiac hypertrophy through regulating HOXA9. Eur. Rev. Med. Pharmacol. Sci. *23*, 281–286.

Yang, D., Li, J., and Yuan, Z. (2013). Gene expression analysis in cardiac tissues from infants identifies candidate agents for Tetralogy of Fallot. Pediatr. Cardiol. *34*, 1637–1644.

Zhang, J., Chang, J.J., Xu, F., Ma, X.J., Wu, Y., Li, W.C., Wang, H.J., Huang, G.Y., and Ma, D. (2013). MicroRNA deregulation in right ventricular outflow tract myocardium in nonsyndromic tetralogy of fallot. Can J. Cardiol. *29*, 1695–1703.

Zhang, J., Muise, E., Han, S., Kutchukian, P., Costet, P., Zhu, Y., Kan, Y., Zhou, H., Shah, V., and Huang, Y. (2020). Molecular profiling reveals a common metabolic signature of tissue fibrosis. Cell Rep. Med. *1*, 100056.

Zhang, J., Qiao, C., Chang, L., Guo, Y., Fan, Y., Villacorta, L., Chen, Y.E., and Zhang, J. (2016). Cardiomyocyte overexpression of FABP4 aggravates pressure overload-induced heart hypertrophy. PLoS One *11*, e0157372.

Zhou, G., Li, C., Feng, J., Zhang, J., and Fang, Y. (2018). lncRNA UCA1 is a novel regulator in cardiomyocyte hypertrophy through targeting the miR-184/HOXA9 axis. Cardiorenal. Med. *8*, 130–139.

Zhou, H., Wang, B., Yang, Y.X., Jia, Q.J., Zhang, A., Qi, Z.W., and Zhang, J.P. (2019). Long noncoding RNAs in pathological cardiac remodeling: a review of the update literature. Biomed. Res. Int. *2019*, 7159592.

iScience, Volume *24*

Supplemental information

RNA expression profiles and regulatory networks in human right ventricular hypertrophy due to high pressure load

Philippe Chouvarine, Joachim Photiadis, Robert Cesnjevar, Jens Scheewe, Ulrike M.M. Bauer, Thomas Pickardt, Hans-Heiner Kramer, Sven Dittrich, Felix Berger, and Georg Hansmann

SUPPLEMENTAL MATERIALS

SUPPLEMENTAL FIGURES

TOF/PS (n=19) vs. VSD controls (n=8) excluding age- and sex-specific genes

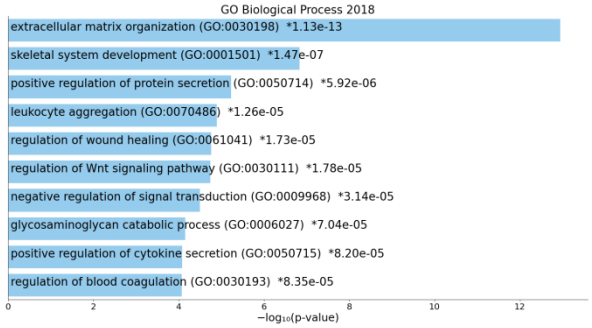

TOF/PS male (n=12) vs. VSD control male (n=3)

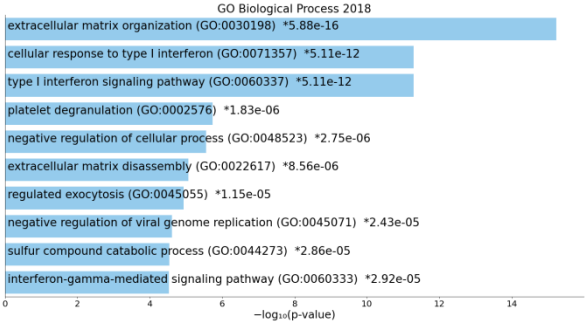

TOF/PS female (n=7) vs. VSD control female (n=5)

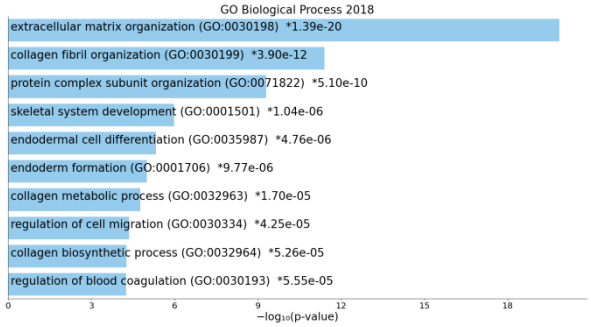

TOF/PS young (n=5) vs. VSD control young (n=3). Young = 2 - 4 months

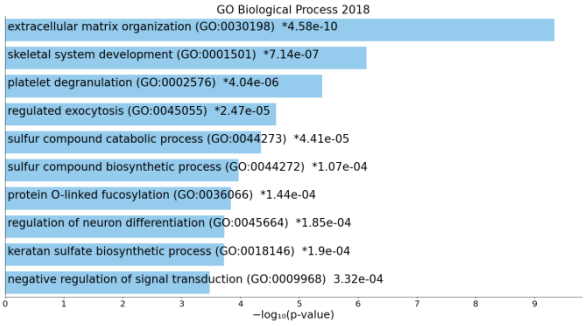

TOF/PS older (n=5) vs. VSD control older (n=4). Older = 7 - 8 months

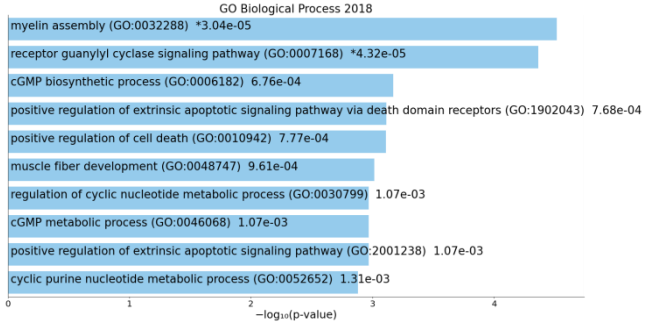

TOF/PS older female (n=2) vs. VSD control older female (n=3). Older = 7 - 8 months

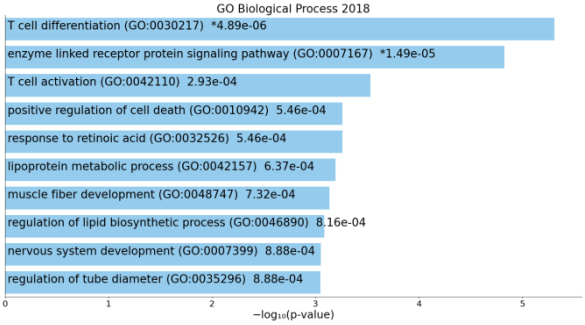

Figure S1. Comparison of top GO biological process terms overrepresented by DEGs among the subgroups shows that age and sex have significant effects on the RVH-associated gene expression profile. Related to Figure 1. The bar charts show the top 10 enriched terms, along with their corresponding p-values (Fisher exact test). An asterisk (*) next to a p-value indicates the term also has a significant adjusted p-value (<0.05). The charts were generated using the Enrichr website (https://maayanlab.cloud/Enrichr/).

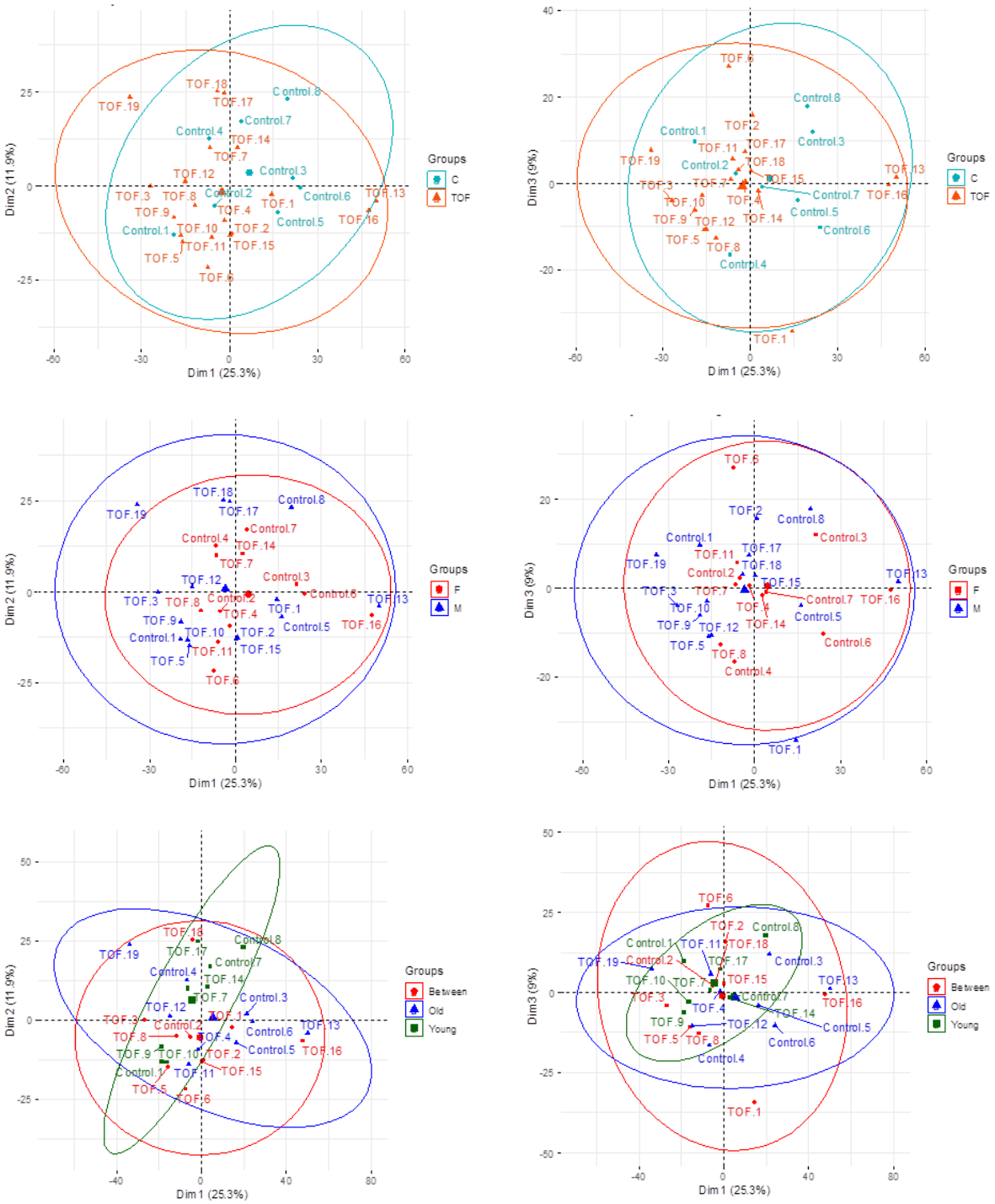

Figure S2 PCA clustering of the patients based on gene expression shows absence of outliers and the effects of RVH-associated expression profile (row 1), sex (row 2), and age (row 3). Related to Figure 1. The age ranges were defined as: young (2 – 4 months), between (5 – 6 months), and old (7 – 8 months).

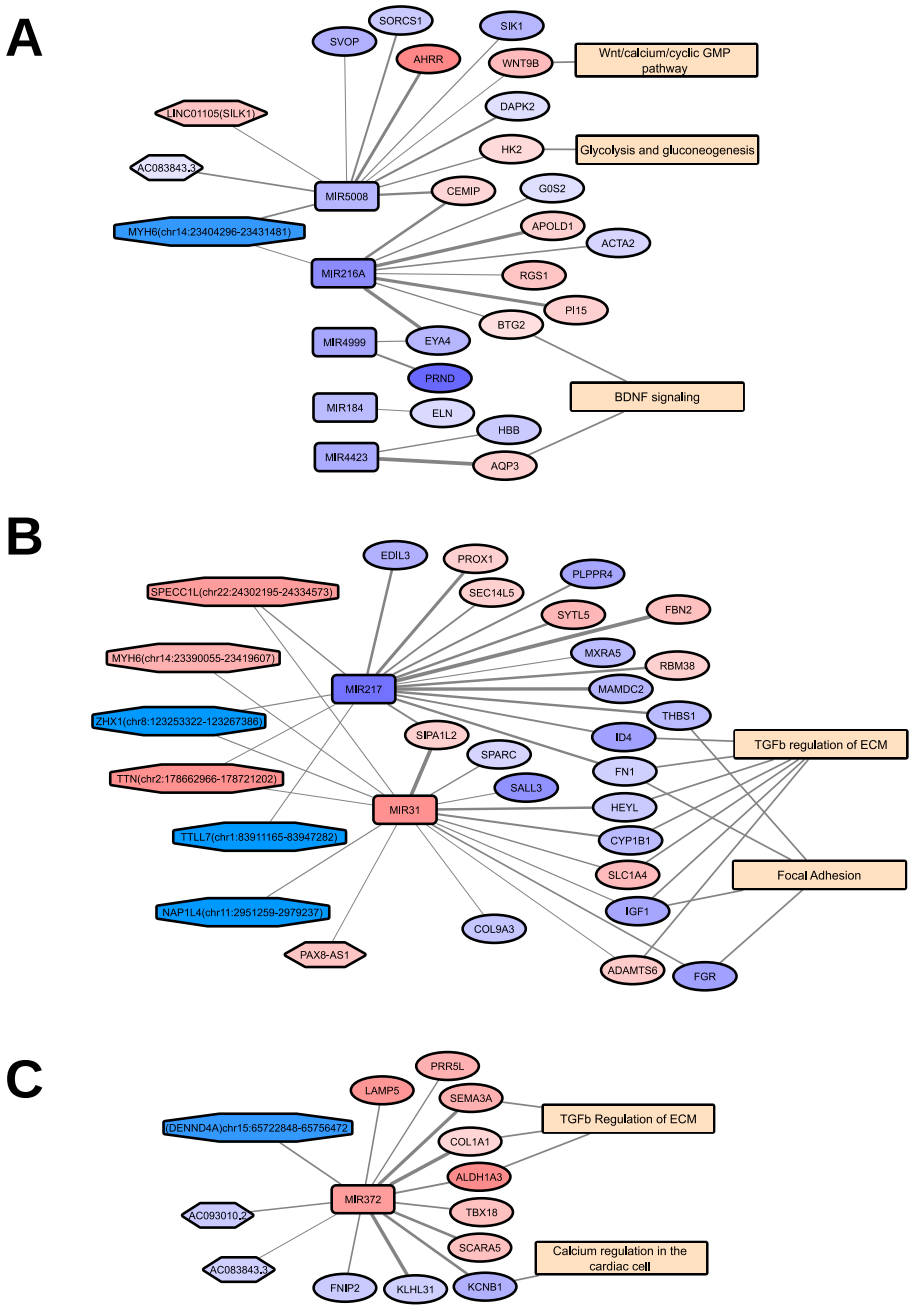

Figure S3 Competing endogenous RNA regulates DEGs and their functions associated with cardiac hypertrophy. Related to Figure 3.

(A) Epigenetic regulation network based on the predicted interactions among differentially expressed molecules of the older group (7-8 months; N_{TOF}=19, N_{Con}=8)), **(B)** The same type of an interaction network for the male group (N_{TOF}=2, N_{Con}=3). **(C)** The same type of an interaction network for the female group (N_{TOF}=2, N_{Con}=3). Nodes are colored blue if downregulated, and red in upregulated. LncRNAs are shown as hexagons, circRNAs are shown as octagons. Line thickness represents the miRNA target score (see Methods). Functional annotation was obtained from the NCATS BioPlanet (https://tripod.nih.gov/bioplanet/).

SUPPLEMENTAL TABLES

Table S1. Demographics data. Related to Figure 1.

Patient ID	Sex	Age, m	Age class	Weight, kg
TOF patients, n = 19	% male: 63	Mean, range: 5.4, (2 - 8)		Mean ± SD: 6.87 ± 0.98
TOF.10	M	2	Young	3.02
TOF.14	F	4	Young	6.35
TOF.15	M	5	Between	6.60
TOF.16	F	6	Between	5.97
TOF.17	M	3	Young	6.30
TOF.18	M	6	Between	6.88
TOF.19	M	7	Older	5.92
TOF.1	M	5	Between	6.87
TOF.2	M	6	Between	7.85
TOF.3	M	6	Between	8.46
TOF.4	F	7	Older	8.30
TOF.5	M	5	Between	7.18
TOF.6	F	5	Between	7.20
TOF.7	F	4	Young	6.79
TOF.8	F	5	Between	5.51
TOF.9	M	4	Young	6.29
TOF.11	F	7	Older	7.80
TOF.12	M	8	Older	8.80
TOF.13	M	7	Older	8.40
VSD controls, n = 8	% male: 37	Mean, range: 6, (1 - 12)		Mean ± SD: 5.59 ± 1.53
Control.3	F	9	Older	5.52
Control.4	F	8	Older	6.15
Control.5	M	7	Older	6.80
Control.6	F	12	Older	8.25
Control.7	F	2	Young	3.71
Control.8	M	4	Young	5.89
Control.1	M	1	Young	4.11
Control.2	F	5	Between	4.27

Table S1. Demographics data. SD = standard deviation of a sample, TOF = tetralogy of Fallot, VSD = ventricular septum defect. Related to Figure 1.

Table S2. Differentially expressed miRNAs separated into subgroups by age and sex. (Related to Figures 2 and 3)

miRNA	Base Mean	Base Mean Control	Base Mean TOF	Fold Change	log2FoldChange	p-val	p-val (adjusted)
TOF/PS (n=19) vs. VSD controls (n=8)							
MIR371A	140.6159	110.5154	212.1047	1.919233	0.94053	0.000211933	0.015541734
MIR372	60.79713	46.78327	94.08003	2.010976	1.007896	0.00019763	0.015541734
MIR31	30.30002	22.40621	49.0478	2.189027	1.13029	6.39E-05	0.009229979
MIR135A2	31.09812	36.23187	18.90548	0.521791	-0.93846	0.000459538	0.028885238
MIR188	75.79432	92.40373	36.34698	0.39335	-1.34612	2.00E-06	0.000439948
MIR216A	21.46441	27.86639	6.259701	0.224633	-2.15436	8.13E-10	3.58E-07
MIR33B	54.08972	64.07841	30.36659	0.473897	-1.07735	8.39E-05	0.009229979
MIR323B	33.67798	38.46429	22.31048	0.580031	-0.7858	0.0008422	0.046321026
TOF/PS male (n=12) vs. VSD control male (n=3)							
MIR31	43.18311	29.75885	96.88014	3.255507	1.702882	0.000305649	0.049820787
MIR217	22.29178	26.41344	5.805148	0.21978	-2.18587	5.64E-05	0.018374094
TOF/PS female (n=7) vs. VSD control female (n=5)							
MIR372	61.69533	37.76899	95.19221	2.52038	1.333641	0.000278438	0.049840345
TOF/PS young (n=5) vs. VSD control young (n=3). Young = 2 - 4 months							
None							
TOF/PS older (n=5) vs. VSD control older (n=4). Older = 7 - 8 months							
MIR184	26.34922	37.76381	12.08097	0.319909	-1.64427	0.000658776	0.049671709
MIR216A	43.93788	70.31685	10.96417	0.155925	-2.68107	1.44E-10	5.43E-08
MIR5008	66.00694	95.76531	28.80898	0.300829	-1.73298	1.33E-06	0.00016718
MIR4999	39.76665	60.55606	13.77989	0.227556	-2.13571	2.72E-07	5.14E-05
MIR4423	26.80051	39.79768	10.55403	0.265192	-1.91489	0.000257479	0.024267442
TOF/PS older female (n=2) vs. VSD control older female (n=3). Older = 7 - 8 months							
MIR219A1	103.2268	180.4917	51.7169	0.286533	-1.80323	0.000429651	0.049497868
MIR216A	31.15925	66.24891	7.766149	0.117227	-3.09263	0.000207648	0.037895674
MIR33A	2268.489	3484.292	1457.954	0.418436	-1.25692	0.000542442	0.049497868
MIR5008	59.55476	116.1735	21.80894	0.187727	-2.41329	9.88E-05	0.036065996

Table S3. Differentially expressed circRNAs separated into subgroups by age and sex. (Related to Figures 2 and 3)

circRNA	Base Mean	Base Mean Control	Base Mean TOF	Fold Change	log2FoldChange	p-val	p-val (adjusted)
TOF/PS (n=19) vs. VSD controls (n=8)							
ENSG00000171517:LPAR3:chr1:84865385:84866138	27.26357	38.74297	0	0	NA	9.87E-24	8.26E-21
ENSG00000155657:TTN:chr2:178693922:178715774	65.40397	45.10203	113.6211	2.519201	1.332966	0.000111	0.046415
ENSG00000127914:AKAP9:chr7:92065231:92101056	76.08315	53.67551	129.3013	2.408943	1.2684	0.000175	0.04886
TOF/PS male (n=12) vs. VSD control male (n=3)							
ENSG00000197616:MYH6:chr14:23390055:23419607	509.1048	405.9485	921.7301	2.270559	1.183047	0.000579	0.04944
ENSG00000235050:MLIP-AS1:chr6:54059858:54063911	79.88163	94.6924	20.63858	0.217954	-2.19791	0.000513	0.048195
ENSG00000156011:PSD3:chr8:188676674:18872733	39.77054	47.80774	7.621711	0.159424	-2.64906	0.00027	0.028184
ENSG00000137941:TTLL7:chr1:83911165:83947282	16.10732	20.13414	0	0	NA	1.27E-06	0.000595
ENSG00000109323:MANBA:chr4:102726589:102730736	40.26892	23.91378	105.6895	4.419606	2.143918	4.65E-05	0.006241
ENSG00000205531:NAP1L4:chr11:2951259:2979237	12.07784	15.09731	0	0	NA	6.99E-06	0.001642
ENSG00000155657:TTN:chr2:178662966:178721202	149.7023	104.1283	331.9981	3.188355	1.672812	2.41E-05	0.004522
ENSG00000038427:VCAN:chr5:83537007:83542268	67.91735	82.1326	11.05638	0.134616	-2.89308	3.06E-05	0.004784
ENSG00000113441:LNPEP:chr5:96979138:96986670	15.60016	19.5002	0	0	NA	2.89E-06	0.000904
ENSG00000165156:ZHX1:chr8:123253322:123267386	42.78134	53.47667	0	0	NA	1.22E-11	1.15E-08
ENSG00000100014:SPECC1L:chr22:24302195:24334573	54.9853	39.71626	116.0614	2.922265	1.547087	0.000202	0.023742
TOF/PS female (n=7) vs. VSD control female (n=5)							
ENSG00000174485:DENND4A:chr15:65722848:65756472	13.62362	21.94164	1.978398	0.090166	-3.47127	1.55E-05	0.030993
TOF/PS young (n=5) vs. VSD control young (n=3). Young = 2 - 4 months							
ENSG00000023287:RB1CC1:chr8:52656008:52686967	59.97058	88.62379	12.21522	0.137832	-2.85901	6.30E-05	0.014566
ENSG00000131023:LATS1:chr6:149676260:149681523	27.5332	8.540755	59.18728	6.929982	2.792852	3.19E-05	0.010319
ENSG00000181192:DHTKD1:chr10:12081472:12091684	11.29966	18.07946	0	0	#NAME?	1.40E-05	0.00756
ENSG00000116984:MTR:chr1:236824119:236853088	23.79878	38.07804	0	0	#NAME?	3.69E-09	2.98E-06
ENSG00000183826:BTBD9:chr6:38577600:38598121	22.77154	35.1382	2.160427	0.061484	-4.02365	2.63E-05	0.010319
ENSG00000115464:USP34:chr2:61325375:61350693	21.67891	33.48962	1.994389	0.059552	-4.0697	4.80E-05	0.012938
ENSG00000034677:RNF19A:chr8:100259107:100288267	22.77834	36.44534	0	0	#NAME?	1.12E-09	1.82E-06
TOF/PS older (n=5) vs. VSD control older (n=4). Older = 7 - 8 months							
ENSG00000197616:MYH6:chr14:23404296:23431481	6533.956	11620.33	175.9837	0.015144	-6.04507	1.94E-18	3.96E-15
TOF/PS older female (n=2) vs. VSD control older female (n=3). Older = 7 - 8 months							
ENSG00000151067:CACNA1C:chr12:2448976:2512984	29.60712	4.738037	46.1865	9.748025	3.28511	8.26E-04	0.049937
ENSG00000137145:DENND4C:chr9:19286769:19300331	24.90189	2.793135	39.64106	14.19232	3.827038	2.39E-04	0.02524

ENSG00000036448:MYOM2:chr8:2052158:2085390	68.6232	140.7586	20.53292	0.145873	-2.77721	6.09E-05	0.012891
ENSG00000078674:PCM1:chr8:18013578:18062423	123.5063	225.8464	55.27957	0.244766	-2.03052	5.44E-04	0.045982
ENSG00000081377:CDC14B:chr9:96509673:96565483	84.00905	21.58439	125.6255	5.820201	2.541069	8.06E-04	0.049937
ENSG00000138162:TACC2:chr10:122082647:122088591	97.94634	186.8081	38.70517	0.207192	-2.27096	2.19E-04	0.02524
ENSG00000183023:SLC8A1:chr2:40428473:40482730	118.423	25.26953	180.5253	7.143991	2.83673	5.92E-05	0.012891

Table S4. Differentially expressed lncRNAs separated into subgroups by age and sex. (Related to Figures 2 and 3)

lncRNA	Base Mean	Base Mean Control	Base Mean TOF	Fold Change	log2FoldChange	p-val	p-val (adjusted)
TOF/PS (n=19) vs. VSD controls (n=8) excluding age-, sex-specific genes (see Methods)							
FAM182A	42.101318	50.377705	22.4449	0.4455324	-1.166398	0.0005128	0.0173232
LINC01405	47.786968	37.761674	71.597043	1.8960241	0.9229773	0.0005004	0.0171207
PAX8-AS1	476.71993	395.95554	668.53536	1.6884102	0.7556654	2.275E-06	0.000205
KANSL1-AS1	134.61881	156.12324	83.545799	0.5351272	-0.902046	7.39E-05	0.0038411
MEG3	3146.2459	3461.6046	2397.2691	0.6925312	-0.530049	2.285E-05	0.001455
LINC02593	100.57567	118.41408	58.209451	0.4915754	-1.024515	2.568E-05	0.0016117
TEX41	63.139467	75.288557	34.28538	0.4553863	-1.134837	6.885E-05	0.0036892
ANKRD10-IT1	101.29123	118.7706	59.777721	0.503304	-0.990498	4.058E-05	0.0023468
LINC01105	56.508895	69.599788	25.418025	0.3652026	-1.453231	1.685E-05	0.0011104
LERFS	56.978117	70.769135	24.224449	0.3423025	-1.546656	7.086E-07	8.02E-05
SOX9-AS1	205.93294	234.98241	136.94045	0.5827689	-0.779004	8.299E-05	0.0042367
LINC02432	64.256807	77.440286	32.946045	0.4254381	-1.232979	4.74E-05	0.0026709
FZD10-AS1	49.135186	59.845582	23.697996	0.3959857	-1.33648	3.175E-05	0.0019112
NAV2-AS2	1188.325	1069.6783	1470.111	1.3743486	0.458748	0.0003338	0.0124529
OVCH1-AS1	77.252891	49.979622	142.0269	2.8416962	1.5067523	3.575E-09	6.668E-07
AL355075.4	310.23202	279.14548	384.06255	1.3758509	0.4603241	0.0019783	0.0497102
AL590004.3	8311.5994	7577.0611	10056.128	1.3271805	0.4083646	0.0006688	0.0216007
CEROX1	212.0316	242.1093	140.59707	0.5807173	-0.784092	3.881E-05	0.002254
AC007952.4	321.42238	279.13082	421.86484	1.5113517	0.5958394	0.0001214	0.00566
KCNQ1OT1	3197.508	3453.7721	2588.8809	0.7495807	-0.415844	0.0011042	0.0320647
RMRP	775.72244	697.33741	961.88688	1.3793708	0.4640104	0.0017015	0.0445287
AC159540.2	62.019335	71.653336	39.138583	0.5462214	-0.872442	0.0012686	0.0358935
BANCR	1173.7777	1059.5895	1444.9747	1.3637118	0.4475388	0.0006848	0.0220085
AL033543.1	136.92748	154.42988	95.359279	0.6174924	-0.695507	0.0015758	0.042133
HELLPAR	67.213478	78.244656	41.014429	0.5241819	-0.931861	0.0005296	0.017816
TOF/PS male (n=12) vs. VSD control male (n=3)							
PAX8-AS1	601.22943	517.86302	934.69508	1.8049079	0.8519253	0.0002715	0.0136216
KANSL1-AS1	136.42173	154.15323	65.495702	0.424874	-1.234893	0.0013004	0.044133
SLC9A3-AS1	319.13123	268.43316	521.92353	1.9443333	0.9592755	0.0001239	0.0076174
LINC01105	60.841458	73.579371	9.8898036	0.13441	-2.895288	1.5E-06	0.0001885
OVCH1-AS1	86.162029	44.983532	250.87601	5.5770635	2.4795057	2.182E-12	1.782E-09
AC020909.2	172.17692	139.12424	304.38761	2.1878833	1.1295358	0.000349	0.0165202
AC100803.4	1620.9442	1445.1562	2324.0964	1.6081974	0.6854445	0.0005147	0.0218037
LOC102724843	64.775079	78.23184	10.948036	0.1399435	-2.837084	4.293E-07	6.546E-05
TOF/PS female (n=7) vs. VSD control female (n=5)							
CYTOR	134.71914	95.059491	190.24265	2.0013009	1.0009381	0.000511	0.0276028
SLC9A3-AS1	311.47726	373.53397	224.59787	0.6012783	-0.733895	0.0008533	0.0414139
LINC00702	163.28498	106.90789	242.21292	2.2656226	1.1799075	5.053E-06	0.0006539
LERFS	44.763262	70.749547	8.3824638	0.1184808	-3.077275	1.342E-09	5.379E-07

AC007126.1	500.61722	595.15744	368.26092	0.6187622	-0.692543	0.0009124	0.0432675
OVCH1-AS1	67.101789	43.25646	100.48525	2.3230114	1.2159962	0.0008863	0.0423514
AC083843.3	1535.9565	1800.8023	1165.1724	0.6470296	-0.628096	0.0007808	0.0381908
AC093010.2	550.64182	657.62571	400.86437	0.6095631	-0.714153	0.0004245	0.0236523
AC007952.4	289.33402	213.6317	395.31727	1.8504617	0.8878852	2.095E-05	0.0019279
TOF/PS young (n=5) vs. VSD control young (n=3). Young = 2 - 4 months							
LINC01405	52.092105	27.173554	93.623023	3.4453728	1.7846601	7.992E-05	0.0048611
PAX8-AS1	447.00115	208.68356	844.19714	4.0453457	2.016263	6.122E-12	2.927E-09
C1RL-AS1	200.52046	253.49232	112.23404	0.4427513	-1.175432	0.0005458	0.0224859
KANSL1-AS1	105.01419	139.28314	47.899273	0.3438986	-1.539945	0.0004421	0.0191476
MEG3	4335.3272	5296.269	2733.7576	0.5161667	-0.954091	1.599E-05	0.0012238
LINC02593	154.60453	198.3916	81.62608	0.4114392	-1.281249	0.0008105	0.0297193
AC025165.1	98.006655	52.192148	174.36417	3.3408122	1.7401989	7.885E-06	0.0006943
LINC00511	52.844233	81.250912	5.4997678	0.0676887	-3.884941	2.891E-09	6.636E-07
LINC00702	172.24773	123.5161	253.46711	2.0520978	1.0370995	0.000807	0.0296868
AL021392.1	347.18267	250.31359	508.63115	2.0319758	1.0228832	0.0001765	0.0090832
FZD10-AS1	80.078213	110.07818	30.078273	0.2732446	-1.871735	0.0001417	0.0077436
OVCH1-AS1	145.6716	60.533521	287.5684	4.7505645	2.248099	8.512E-10	2.272E-07
AL590004.3	6355.5204	4377.6622	9651.9507	2.2048185	1.1406599	1.231E-07	1.935E-05
CEROX1	295.09013	375.8238	160.53402	0.4271523	-1.227177	0.0001452	0.0078994
AC021087.4	970.03803	692.27026	1432.9843	2.0699782	1.0496156	1.973E-05	0.0014513
LINC01896	41.172052	60.0653	9.6833044	0.161213	-2.63296	7.978E-05	0.0048611
AC100803.4	1510.9083	1108.0579	2182.3258	1.9695053	0.9778333	2.521E-05	0.0018085
AC159540.2	90.58523	119.80016	41.893684	0.3496964	-1.515825	0.0003236	0.0151594
TOF/PS older (n=5) vs. VSD control older (n=4). Older = 7 - 8 months							
KANSL1-AS1	187.72998	247.56953	112.93053	0.4561568	-1.132398	0.0001799	0.0188502
LINC01359	238.74259	168.77596	326.20089	1.932745	0.9506513	0.0003258	0.0292985
LINC01105	102.04952	61.084693	153.25556	2.5089029	1.3270566	0.000561	0.0467671
LINC02432	67.265575	34.267556	108.5131	3.1666425	1.662954	0.0002001	0.0198824
AC083843.3	2049.1323	1610.4377	2597.5006	1.612916	0.6896713	0.0004481	0.0381914
AL590004.3	7562.4842	5129.5752	10603.62	2.0671537	1.0476457	4.944E-10	3.529E-07
AC007952.4	237.20709	145.69915	351.592	2.4131369	1.2709098	2.219E-06	0.000497
AP005131.6	547.70438	418.30588	709.45251	1.6960137	0.7621478	0.0006238	0.0494752
AC018645.3	113.25587	162.84406	51.270625	0.3148449	-1.667287	2.099E-06	0.0004793
LOC102724951	180.91927	309.0633	20.739228	0.0671035	-3.897468	1.293E-30	1.476E-26
LOC102724843	76.351169	121.13632	20.36973	0.1681554	-2.572133	6.686E-10	4.019E-07
TOF/PS older female (n=2) vs. VSD control older female (n=3). Older = 7 - 8 months							
PAX8-AS1	349.61397	169.94349	469.39429	2.762061	1.4657452	2.72E-06	0.0006491
NUTM2B-AS1	809.04021	1141.9033	587.13151	0.5141692	-0.959685	0.000147	0.0191043
LERFS	84.853942	22.814046	126.21387	5.5322882	2.4678763	8.566E-06	0.0016537
NEAT1	29745.24	40744.744	22412.236	0.5500645	-0.862327	6.824E-05	0.0104172
LINC02208	150.56321	273.45302	68.636673	0.2509999	-1.994241	1.501E-06	0.0004106
AL121839.2	55.969981	106.92775	21.998137	0.205729	-2.281183	9.484E-05	0.0139895
FP236241.2	83.873095	17.893181	127.8597	7.1457223	2.8370798	9.851E-08	3.919E-05

Table S5. Clusters of DEGs built around the "hub" genes based on their co-expression and the corresponding pathways overrepresented by the DEGs from such clusters. Related to Figure 1. Note: Only the clusters of DEGs that were significantly over-represented in pathways are shown.

Term	Overlap	P-value	Adjusted P-value	Odds Ratio	Genes
KCNMA1 cluster (prominent in VSD controls, faint in TOF/PS) ***TOF/PS genes***: KCNMA1, MATN4 **(No significantly overrepresented pathways)** ***VSD control genes:*** ACTA2, AHNAK2, BICC1, CCDC3, CCDC80, COL14A1, COL5A1, COL8A1, CPXM2, CPZ, CRISPLD1, CTGF, DPYSL3, ECM1, ELN, ENSG00000280143, ENSG00000283378, FN1, GAP43, HEYL, HTR2A, IGF1, KCNJ2, KCNMA1, LOX, MMP19, MXRA8, MYH11, MYLK, MYO1D, MYRF, NKD1, NLGN2, NNMT, NTRK2, OSR1, PLXDC2, POSTN, PRSS23, PTPRZ1, RAB31, RHBDF2, SCARF2, SCRG1, SLC17A9, SLN, SOD3, TAGLN ***Differentially expressed miRNAs targeting mRNA of multiple DEGs in the cluster:*** miR371A (FC=1.91) targets COL14A1 (FC=0.70) and PLXDC2 (FC=0.75) miR372 (FC=2.01) targets CPXM2 (FC=0.51), MYLK (FC=0.73), and MYRF (FC=0.35) ***Differentially expressed lncRNAs targeting mRNA of multiple DEGs in the cluster:*** BANCR (FC=1.36) targets MATN4 (FC=0.29) and MXRA8 (FC=0.69) HELLPAR (FC=0.52) targets MYRF (FC=0.35) and NLGN2 (FC=0.58) **VSD control pathways (adj_p-val <0.05):**					
TGF-beta regulation of extracellular matrix	10/565	7.44E-07	0.001123	7.374631	ACTA2;HEYL;POSTN;LOX;ELN;FN1;IGF1;SOD3;SCRG1;CTGF
Smooth muscle contraction	3/22	1.93E-05	0.014608	56.81818	ACTA2;MYH11;MYLK
Integrins in angiogenesis	4/74	2.97E-05	0.014948	22.52252	COL5A1;COL14A1;FN1;COL8A1
THBS3 cluster (prominent in TOF/PS, faint in VSD controls) ***TOF/PS genes***: ACAN, ADAMTS10, ADAMTSL2, AEBP1, AHNAK2, BCAT1, BGN, BICC1, BOC, CCDC80, CFB, CHST6, COL8A1, COL8A2, CRISPLD1, CTSK, DCLK1, DSEL, EDIL3, ENSG00000260807, FAP, FBLN7, FIBIN, FKBP10, FMOD, GAP43, HTR2A, IGF1, ITGA11, LAMP5, LTBP2, MAPK10, MMP19, MXRA5, MYLK, MYO1D, NRCAM, NTM, PCOLCE, PLPPR4, PLXDC1, PLXDC2, PLXNB3, PRUNE2, RNF112, RYR3, SALL3, SCARA3, SCARA5, SCRG1, SERPINF1, SETBP1, SLC16A4, SLN, SOX8, SPARC, SSC5D, SULF1, TAGLN, TEX41, TGFB3, THBS3, TPBG, TTC39B, UCHL1, VCAN, WFDC1 ***VSD control genes:*** ADAM33, ADAMTS10, AEBP1, ARHGDIG, BCAT1, BOC, BRSK2, C18orf54, C1QTNF6, CEP126, CHST6, COL8A2, CPT1C, DKK2, DNM1, ENSG00000223764, ENSG00000260807, F2RL1, FMOD, FZD10-AS1, HELLPAR, HHIPL1, HMCN1, HTR2B, IGF1, INHBA, ITGA11, ITGA8, MAPK10, NRXN2, OLFML2B, RHOU, SAMD11, SCARA3, SCRG1, SETBP1, SSC5D, SULF1, THBS3, TPBG, TRABD2B, TRAF5, UNC5C, VCAN, WFDC1, ZNF469 **(No significantly overrepresented pathways)** ***Differentially expressed miRNAs targeting mRNA of multiple DEGs in the cluster:*** miR371A (FC=1.91) targets PLXDC2 (FC=0.75) and RHOU (FC=0.49) miR372 (FC=2.01) targets C18orf54 (FC=0.63), CEP126 (FC=0.60), LAMP5 (FC=0.21), MYLK (FC=0.73), and SCARA5 (FC=0.64) ***Differentially expressed lncRNAs targeting mRNA of multiple DEGs in the cluster:*** BANCR (FC=1.36) targets FAP (FC=0.60) and SETBP1 (FC=0.69) **TOF/PS pathways (adj_p-val <0.05):**					
TGF-beta regulation of extracellular matrix	11/565	2.54E-06	3.84E-03	5.81165	UCHL1;VCAN;CTSK;ITGA11;COL8A2;NRCAM;LTBP2;AEBP1;IGF1;SCRG1;CFB
Glycosaminoglycan metabolism	5/110	3.38E-05	2.55E-02	13.56852	ACAN;CHST6;VCAN;BGN;FMOD
Keratan sulfate/keratin metabolism	3/31	1.51E-04	7.60E-02	28.88782	ACAN;CHST6;FMOD
FKBP10 cluster (prominent in TOF/PS, faint in VSD controls) ***TOF/PS genes***: ADAMTS2, AEBP1, BGN, BOC, CCDC80, CEP126, CHST2, CLEC11A, COL14A1, COL1A2, COL5A1, DNM1, DPYSL3, ECM1, EDIL3, ELN, FBLN1, FBLN7, FKBP10, FMOD, FN1, HHIPL1, IGF1, ITGA11, LTBP2, MRC2, MRVI1, MXRA5, MXRA8, MYLK, MYO1D, MYRF, OLFML2B, PCOLCE, PLXDC2, PLXNB3, RAB31, RCN3, RUNX1, SALL3, SESN3, SFRP4, SPARC, SSC5D, TAGLN, THBS2, THBS3, TNC, UNC5C ***VSD control genes:*** CLEC11A, COL8A2, CTSK, FKBP10, ITGA11, LAMP5, LTBP2, NTM, PLPPR4, PRUNE2, RCN3, SFRP4, SLC16A4, TGFB3, THBS2 ***Differentially expressed miRNAs targeting mRNA of multiple DEGs in the cluster:*** miR31 (FC=2.19) targets SALL3 (FC=0.30) and SPARC (FC=0.68) miR371A (FC=1.91) targets COL14A1 (FC=0.70), MRVI1 (FC=0.68), and PLXDC2 (FC=0.75) miR372 (FC=2.01) targets CEP126 (FC=0.60), LAMP5 (FC=0.21), MYLK (FC=0.73), and MYRF (FC=0.35)					

Differentially expressed lncRNAs targeting mRNA of multiple DEGs in the cluster:
BANCR (FC=1.36) targets CLEC11A(FC=0.65) and MXRA8 (FC=0.69)

TOF/PS pathways (adj_p-val <0.05):

ECM-receptor interaction	7/84	1.33E-09	2.01E-06	34.01361	COL1A2;COL5A1;ITGA11;TNC;FN1;THBS2;THBS3
Focal adhesion	9/233	4.64E-09	3.50E-06	15.76596	COL1A2;COL5A1;ITGA11;TNC;FN1;IGF1;THBS2;MYLK;THBS3
Beta-1 integrin cell surface interactions	6/66	1.28E-08	6.44E-06	37.10575	COL1A2;COL5A1;ITGA11;TNC;FN1;THBS2
TGF-beta regulation of extracellular matrix	11/565	9.13E-08	3.45E-05	7.946541	SFRP4;COL1A2;ELN;ITGA11;TNC;FN1;FBLN1;LTBP2;AEBP1;IGF1;THBS2
Collagen biosynthesis and modifying enzymes	5/64	4.89E-07	1.48E-04	31.88776	ADAMTS2;COL1A2;COL5A1;COL14A1;PCOLCE
Integrins in angiogenesis	5/74	1.02E-06	2.56E-04	27.5786	COL1A2;COL5A1;COL14A1;FN1;EDIL3
Extracellular matrix organization	5/93	3.16E-06	6.82E-04	21.94426	ADAMTS2;COL1A2;COL5A1;COL14A1;PCOLCE
Beta-3 integrin cell surface interactions	4/43	3.66E-06	6.90E-04	37.96868	COL1A2;TNC;FN1;EDIL3
Inflammatory response pathway	3/30	5.36E-05	0.008985	40.81633	COL1A2;FN1;THBS3
Integrin cell surface interactions	4/85	5.56E-05	0.008401	19.20768	COL1A2;ITGA11;TNC;FN1
Developmental biology	7/420	6.87E-05	0.009436	6.802721	COL1A2;COL5A1;BOC;DPYSL3;PLXNB3;UNC5C;DNM1
Small leucine-rich proteoglycan (SLRP) molecules	2/6	8.76E-05	0.011029	136.0544	BGN;FMOD
Axon guidance	6/325	1.37E-04	0.015855	7.535322	COL1A2;COL5A1;DPYSL3;PLXNB3;UNC5C;DNM1
Syndecan 1 pathway	3/46	1.95E-04	0.02101	26.61934	COL1A2;COL5A1;COL14A1
Signaling by PDGF	4/122	2.26E-04	0.022734	13.3824	COL1A2;COL5A1;THBS2;THBS3

VSD control pathways (adj_p-val <0.05):

TGF-beta regulation of extracellular matrix	6/565	1.99E-06	0.00301	14.15929	SFRP4;CTSK;ITGA11;COL8A2;LTBP2;THBS2

BGN cluster (prominent in TOF/PS, faint in VSD controls)

TOF/PS genes: ACAN, ADAMTS10, ADAMTS2, ADAMTSL2, AEBP1, AHNAK2, ALDH1A3, BCAT1, BGN, BICC1, BOC, CCDC80, CFB, CHST2, CHST6, CLEC11A, COL14A1, COL1A2, COL5A1, COL8A1, COL8A2, CTSK, DCLK1, DNM1, DPYSL3, DSEL, EDIL3, ELN, CEROX1, F2RL1, FBLN1, FBLN7, FIBIN, FKBP10, FMOD, FN1, GAP43, HHIPL1, HTR2A, HTR4, IGF1, ITGA11, LAMP5, LTBP2, MAPK10, MMP19, MRC2, MRVI1, MXRA5, MXRA8, MYLK, MYO1D, MYRF, NKD1, NLGN2, NRXN2, OLFML2B, PCOLCE, PLXDC1, PLXDC2, PLXNB3, PRTFDC1, PRUNE2, RAB31, RCN3, RNF112, RYR3, SALL3, SCARA3, SCARA5, SCRG1, SERPINF1, SESN3, SETBP1, SFRP4, SLC16A4, SLN, SOX8, SPARC, SSC5D, SULF1, TAGLN, TEX41, TGFB3, THBS2, THBS3, TNC, TPBG, TRAF5, TTC39B, VCAN, WFDC1

VSD control genes: ADAMTS2, ADAMTSL2, BGN, COL5A1, CPXM2, CRISPLD1, ELN, FNDC1, GPC6, HIST3H2A, HTR4, IGF1, LOX, LRRC17, MICALL2, MMP19, MXRA8, NLGN2, PCOLCE, PRELP, RAB31, SCARF2, SCRG1, SLN, TAGLN, TIMP1, TMEM100

Differentially expressed miRNAs targeting mRNA of multiple DEGs in the cluster:
miR31 (FC=2.19) targets SALL3 (FC=0.30) and SPARC (FC=0.68)
miR371A (FC=1.91) targets COL14A1 (FC=0.70), GPC6 (FC=0.70), MRVI1 (FC=0.68), PLXDC1 (FC=0.70), and PLXDC2 (FC=0.75)
miR372 (FC=2.01) targets ALDH1A3 (FC=0.48), CPXM2 (FC=0.51), GPC6 (FC=0.70), LAMP5 (FC=0.21), MYLK (FC=0.73), MYRF (FC=0.35), and SCARA5 (FC=0.63)

Differentially expressed lncRNAs targeting mRNA of multiple DEGs in the cluster:
BANCR (FC=1.36) targets CLEC11A, MXRA8 (FC=0.69), and SETBP1 (FC=0.69)
HELLPAR (FC=0.52) targets MYRF (FC=0.35) and NLGN2 (FC=0.58)

TOF/PS pathways (adj_p-val <0.05):

TGF-beta regulation of	17/565	7.25E-10	1.09E-06	6.540977	ELN;TNC;FN1;FBLN1;LTBP2;AEBP1;IGF1;THBS2;ALDH1A3;SFRP4;VCAN;COL1A2;CTSK;ITGA11;COL8A2;SCRG1;CFB

extracellular matrix					
Collagen biosynthesis and modifying enzymes	7/64	1.73E-08	1.31E-05	23.77717	ADAMTS2;COL1A2;COL5A1;COL14A1;COL8A2;COL8A1;PCOLCE
Integrins in angiogenesis	7/74	4.84E-08	2.44E-05	20.56404	COL1A2;COL5A1;COL14A1;COL8A2;FN1;COL8A1;EDIL3
ECM-receptor interaction	7/84	1.17E-07	4.43E-05	18.11594	COL1A2;COL5A1;ITGA11;TNC;FN1;THBS2;THBS3
Focal adhesion	10/233	1.19E-07	3.59E-05	9.330099	MAPK10;COL1A2;COL5A1;ITGA11;TNC;FN1;IGF1;THBS2;MYLK;THBS3
Extracellular matrix organization	7/93	2.37E-07	5.98E-05	16.36279	ADAMTS2;COL1A2;COL5A1;COL14A1;COL8A2;COL8A1;PCOLCE
Beta-1 integrin cell surface interactions	6/66	5.84E-07	1.26E-04	19.76285	COL1A2;COL5A1;ITGA11;TNC;FN1;THBS2
Syndecan 1 pathway	5/46	2.18E-06	4.11E-04	23.62949	COL1A2;COL5A1;COL14A1;COL8A2;COL8A1
Glycosaminoglycan metabolism	6/110	1.17E-05	0.001966	11.85771	ACAN;CHST6;VCAN;BGN;FMOD;CHST2
Keratan sulfate/keratin metabolism	4/31	1.20E-05	0.001811	28.05049	ACAN;CHST6;FMOD;CHST2
Beta-3 integrin cell surface interactions	4/43	4.51E-05	0.006191	20.22245	COL1A2;TNC;FN1;EDIL3
Small leucine-rich proteoglycan (SLRP) molecules	2/6	3.10E-04	0.039034	72.46377	BGN;FMOD
Inflammatory response pathway	3/30	3.49E-04	0.040596	21.73913	COL1A2;FN1;THBS3
VSD control pathways (adj_p-val <0.05):					
Extracellular matrix organization	4/93	7.08E-06	0.010696	31.85982	ADAMTS2;COL5A1;PCOLCE;TIMP1

SALL3 cluster (prominent in TOF/PS, faint in VSD controls)

TOF/PS genes: ACAN, ADAMTS10, ADAMTSL2, AEBP1, ALDH1A3, BGN, BICC1, BOC, CCDC80, CHST6, CLDN11, COL8A2, CTSK, DCLK1, DSEL, EDIL3, CEROX1, F2RL1, FBLN7, FKBP10, FMOD, HTR4, ID4, IGF1, ITGA11, ITGA8, LTBP2, MAPK10, MXRA5, MYLK, MYO1D, NKD1, NRXN2, PCOLCE, PLXDC2, PLXNB3, PRTFDC1, PTPRZ1, RNF112, RYR3, SALL3, SCARA5, SCRG1, SETBP1, SLC16A4, SPARC, SSC5D, TAGLN, TEX41, THBS3, TPBG, TRAF5, TTC39B, VCAN

VSD control genes: ARHGDIG, BRSK2, C18orf54, CHST2, CHST6, CLDN11, COL8A2, CPT1C, DKK2, DNM1, FZD10-AS1, HHIPL1, HTR2B, IGF1, ITGA11, ITGA2, KCNK17, MATN4, MIR323B, NRXN2, SALL3, SAMD5, SCRG1, SESN3, SSC5D **(No significantly overrepresented pathways)**

Differentially expressed miRNAs targeting mRNA of multiple DEGs in the cluster:

miR31 (FC=2.19) targets SALL3 (FC=0.30) and SPARC (FC=0.68)

miR372 (FC=2.01) targets ALDH1A3 (FC=0.48), C18orf54 (FC=0.63), MYLK (FC=0.73), and SCARA5 (FC=0.63)

Differentially expressed lncRNAs targeting mRNA of multiple DEGs in the cluster:

BANCR (FC=1.36) targets MATN4 (FC=0.29) and SETBP1 (FC=0.69)

TOF/PS pathways (adj_p-val <0.05):

TGF-beta regulation of extracellular matrix	10/565	2.34E-06	0.003529	6.555228	ALDH1A3;VCAN;CTSK;ITGA11;COL8A2;ID4;LTBP2;AEBP1;IGF1;SCRG1
Glycosaminoglycan metabolism	5/110	1.17E-05	0.008847	16.83502	ACAN;CHST6;VCAN;BGN;FMOD
Focal adhesion	6/233	3.79E-05	0.019097	9.537434	MAPK10;ITGA11;ITGA8;IGF1;MYLK;THBS3
Keratan sulfate/keratin metabolism	3/31	7.93E-05	0.029924	35.84229	ACAN;CHST6;FMOD
Small leucine-rich proteoglycan (SLRP) molecules	2/6	1.07E-04	0.032188	123.4568	BGN;FMOD

Table S6. Differentially expressed lncRNAs targeting DNA of DEGs in the co-expression clusters. Related to Figure 1.

Note: The complete list of lncRNA targets is presented in Table S6. The co-expression clusters are defined in Table S5.

Interactor1	Category1	FoldChange1	Interactor2	Category2	FoldChange2
KCNMA1 cluster (prominent in VSD controls, faint in TOF/PS)					
MEG3	lncRNA	0.69	IGF1	DNA	0.43
MEG3	lncRNA	0.69	KCNMA1	DNA	0.37
MEG3	lncRNA	0.69	BICC1	DNA	0.72
MEG3	lncRNA	0.69	COL14A1	DNA	0.70
MEG3	lncRNA	0.69	CPXM2	DNA	0.51
MEG3	lncRNA	0.69	ELN	DNA	0.39
MEG3	lncRNA	0.69	HTR2A	DNA	0.34
MEG3	lncRNA	0.69	SCRG1	DNA	0.21
MEG3	lncRNA	0.69	KCNJ2	DNA	1.36
MEG3	lncRNA	0.69	NTRK2	DNA	0.52
MEG3	lncRNA	0.69	RHBDF2	DNA	0.60
MEG3	lncRNA	0.69	MYH11	DNA	0.62
MEG3	lncRNA	0.69	MYLK	DNA	0.73
MEG3	lncRNA	0.69	PRSS23	DNA	0.69
MEG3	lncRNA	0.69	PLXDC2	DNA	0.75
RMRP	lncRNA	1.41	MATN4	DNA	0.29
RMRP	lncRNA	1.41	CCDC3	DNA	0.69
RMRP	lncRNA	1.41	COL5A1	DNA	0.76
RMRP	lncRNA	1.41	GAP43	DNA	0.37
RMRP	lncRNA	1.41	CPZ	DNA	0.53
RMRP	lncRNA	1.41	FN1	DNA	0.67
RMRP	lncRNA	1.41	KCNMA1	DNA	0.37
RMRP	lncRNA	1.41	MYH11	DNA	0.62
RMRP	lncRNA	1.41	NTRK2	DNA	0.52
THBS3 cluster (prominent in TOF/PS, faint in VSD controls)					
MEG3	lncRNA	0.69	DKK2	DNA	0.45
MEG3	lncRNA	0.69	SALL3	DNA	0.30
MEG3	lncRNA	0.69	SETBP1	DNA	0.69
MEG3	lncRNA	0.69	PLXDC1	DNA	0.70
MEG3	lncRNA	0.69	SCRG1	DNA	0.21
MEG3	lncRNA	0.69	EDIL3	DNA	0.42
MEG3	lncRNA	0.69	VCAN	DNA	0.61
MEG3	lncRNA	0.69	SULF1	DNA	0.67
MEG3	lncRNA	0.69	SAMD11	DNA	0.48
MEG3	lncRNA	0.69	C18orf54	DNA	0.63
MEG3	lncRNA	0.69	UNC5C	DNA	0.63
MEG3	lncRNA	0.69	SETBP1	DNA	0.69
MEG3	lncRNA	0.69	IGF1	DNA	0.43
MEG3	lncRNA	0.69	PLPPR4	DNA	0.50
MEG3	lncRNA	0.69	ITGA11	DNA	0.55
MEG3	lncRNA	0.69	MXRA5	DNA	0.52
MEG3	lncRNA	0.69	HTR2A	DNA	0.34
MEG3	lncRNA	0.69	TRABD2B	DNA	0.38
MEG3	lncRNA	0.69	MYLK	DNA	0.73
MEG3	lncRNA	0.69	NRCAM	DNA	0.48
MEG3	lncRNA	0.69	NTM	DNA	0.46
MEG3	lncRNA	0.69	PLXDC2	DNA	0.75
MEG3	lncRNA	0.69	BOC	DNA	0.62
MEG3	lncRNA	0.69	AEBP1	DNA	0.40
MEG3	lncRNA	0.69	BOC	DNA	0.62
MEG3	lncRNA	0.69	SCRG1	DNA	0.21
MEG3	lncRNA	0.69	DSEL	DNA	0.73
MEG3	lncRNA	0.69	BRSK2	DNA	0.31
MEG3	lncRNA	0.69	INHBA	DNA	0.68
MEG3	lncRNA	0.69	BICC1	DNA	0.72
MEG3	lncRNA	0.69	ADAMTSL2	DNA	0.58

MEG3	lncRNA	0.69	RHOU	DNA	0.49
RMRP	lncRNA	1.41	RHOU	DNA	0.49
RMRP	lncRNA	1.41	SULF1	DNA	0.67
RMRP	lncRNA	1.41	LTBP2	DNA	0.45
RMRP	lncRNA	1.41	EDIL3	DNA	0.42
RMRP	lncRNA	1.41	FMOD	DNA	0.38
RMRP	lncRNA	1.41	FAP	DNA	0.60
RMRP	lncRNA	1.41	RNF112	DNA	0.58
RMRP	lncRNA	1.41	RYR3	DNA	0.25
RMRP	lncRNA	1.41	ITGA11	DNA	0.55
RMRP	lncRNA	1.41	SOX8	DNA	0.61
RMRP	lncRNA	1.41	SAMD11	DNA	0.48
RMRP	lncRNA	1.41	ADAMTS10	DNA	0.70
RMRP	lncRNA	1.41	DNM1	DNA	0.68
RMRP	lncRNA	1.41	GAP43	DNA	0.37
RMRP	lncRNA	1.41	ITGA8	DNA	0.62
RMRP	lncRNA	1.41	BRSK2	DNA	0.31
RMRP	lncRNA	1.41	INHBA	DNA	0.68
RMRP	lncRNA	1.41	ZNF469	DNA	0.69
RMRP	lncRNA	1.41	NTM	DNA	0.46
RMRP	lncRNA	1.41	TGFB3	DNA	0.67
RMRP	lncRNA	1.41	SALL3	DNA	0.30
FKBP10 cluster (prominent in TOF/PS, faint in VSD controls)					
MEG3	lncRNA	0.69	PLPPR4	DNA	0.50
MEG3	lncRNA	0.69	CHST2	DNA	0.53
MEG3	lncRNA	0.69	SESN3	DNA	0.71
MEG3	lncRNA	0.69	MRVI1	DNA	0.68
MEG3	lncRNA	0.69	NTM	DNA	0.46
MEG3	lncRNA	0.69	FBLN1	DNA	0.63
MEG3	lncRNA	0.69	MXRA5	DNA	0.52
MEG3	lncRNA	0.69	ITGA11	DNA	0.55
MEG3	lncRNA	0.69	IGF1	DNA	0.43
MEG3	lncRNA	0.69	UNC5C	DNA	0.63
MEG3	lncRNA	0.69	BOC	DNA	0.62
MEG3	lncRNA	0.69	SALL3	DNA	0.30
MEG3	lncRNA	0.69	MYLK	DNA	0.73
MEG3	lncRNA	0.69	COL14A1	DNA	0.70
MEG3	lncRNA	0.69	PLXDC2	DNA	0.75
MEG3	lncRNA	0.69	ELN	DNA	0.39
MEG3	lncRNA	0.69	AEBP1	DNA	0.40
MEG3	lncRNA	0.69	ADAMTS2	DNA	0.71
MEG3	lncRNA	0.69	EDIL3	DNA	0.42
MEG3	lncRNA	0.69	RUNX1	DNA	0.58
MEG3	lncRNA	0.69	COL1A2	DNA	0.74
RMRP	lncRNA	1.41	LTBP2	DNA	0.45
RMRP	lncRNA	1.41	RUNX1	DNA	0.58
RMRP	lncRNA	1.41	EDIL3	DNA	0.42
RMRP	lncRNA	1.41	LTBP2	DNA	0.45
RMRP	lncRNA	1.41	ITGA11	DNA	0.55
RMRP	lncRNA	1.41	COL5A1	DNA	0.76
RMRP	lncRNA	1.41	TGFB3	DNA	0.67
RMRP	lncRNA	1.41	SALL3	DNA	0.30
RMRP	lncRNA	1.41	DNM1	DNA	0.68
RMRP	lncRNA	1.41	FBLN1	DNA	0.63
RMRP	lncRNA	1.41	NTM	DNA	0.46
RMRP	lncRNA	1.41	THBS2	DNA	0.61
RMRP	lncRNA	1.41	FMOD	DNA	0.38
RMRP	lncRNA	1.41	FN1	DNA	0.67
BGN cluster (prominent in TOF/PS, faint in VSD controls)					
MEG3	lncRNA	0.69	ITGA11	DNA	0.55
MEG3	lncRNA	0.69	SETBP1	DNA	0.69
MEG3	lncRNA	0.69	MRVI1	DNA	0.68
MEG3	lncRNA	0.69	FBLN1	DNA	0.63
MEG3	lncRNA	0.69	CHST2	DNA	0.53
MEG3	lncRNA	0.69	SULF1	DNA	0.67

MEG3	lncRNA	0.69	COL1A2	DNA	0.74
MEG3	lncRNA	0.69	CPXM2	DNA	0.51
MEG3	lncRNA	0.69	PRTFDC1	DNA	0.62
MEG3	lncRNA	0.69	SCRG1	DNA	0.21
MEG3	lncRNA	0.69	SESN3	DNA	0.71
MEG3	lncRNA	0.69	MXRA5	DNA	0.52
MEG3	lncRNA	0.69	HTR2A	DNA	0.34
MEG3	lncRNA	0.69	ALDH1A3	DNA	0.48
MEG3	lncRNA	0.69	MYLK	DNA	0.73
MEG3	lncRNA	0.69	ADAMTS2	DNA	0.71
MEG3	lncRNA	0.69	TMEM100	DNA	0.52
MEG3	lncRNA	0.69	EDIL3	DNA	0.42
MEG3	lncRNA	0.69	IGF1	DNA	0.43
MEG3	lncRNA	0.69	PLXDC1	DNA	0.70
MEG3	lncRNA	0.69	AEBP1	DNA	0.40
MEG3	lncRNA	0.69	BICC1	DNA	0.72
MEG3	lncRNA	0.69	VCAN	DNA	0.61
MEG3	lncRNA	0.69	ADAMTSL2	DNA	0.58
MEG3	lncRNA	0.69	GPC6	DNA	0.70
MEG3	lncRNA	0.69	ELN	DNA	0.39
MEG3	lncRNA	0.69	PLXDC2	DNA	0.75
MEG3	lncRNA	0.69	COL14A1	DNA	0.70
MEG3	lncRNA	0.69	BOC	DNA	0.62
MEG3	lncRNA	0.69	DSEL	DNA	0.73
MEG3	lncRNA	0.69	SALL3	DNA	0.30
RMRP	lncRNA	1.41	MICALL2	DNA	0.71
RMRP	lncRNA	1.41	TGFB3	DNA	0.67
RMRP	lncRNA	1.41	RNF112	DNA	0.58
RMRP	lncRNA	1.41	FMOD	DNA	0.38
RMRP	lncRNA	1.41	EDIL3	DNA	0.42
RMRP	lncRNA	1.41	RYR3	DNA	0.25
RMRP	lncRNA	1.41	SULF1	DNA	0.67
RMRP	lncRNA	1.41	THBS2	DNA	0.61
RMRP	lncRNA	1.41	SALL3	DNA	0.30
RMRP	lncRNA	1.41	SOX8	DNA	0.61
RMRP	lncRNA	1.41	ADAMTS10	DNA	0.70
RMRP	lncRNA	1.41	DNM1	DNA	0.68
RMRP	lncRNA	1.41	ITGA11	DNA	0.55
RMRP	lncRNA	1.41	FBLN1	DNA	0.63
RMRP	lncRNA	1.41	GAP43	DNA	0.37
RMRP	lncRNA	1.41	COL5A1	DNA	0.76
RMRP	lncRNA	1.41	FN1	DNA	0.67
RMRP	lncRNA	1.41	LTBP2	DNA	0.45
SALL3 cluster (prominent in TOF/PS, faint in VSD controls)					
None					

TRANSPARENT METHODS

RESOURCE AVAILABILITY

Lead Contact

Georg Hansmann, Department of Pediatric Cardiology and Critical Care, Hannover Medical School, Carl-Neuberg-Str. 1, 30625 Hannover, Germany. E-mail: georg.hansmann@gmail.com

Materials Availability

Further information and requests for resources and reagents should be directed to and will be fulfilled by the Lead Contact, Georg Hansmann (georg.hansmann@gmail.com), according to the material transfer agreement (MTA). This study did not generate new unique reagents.

Data and Code Availability

This study did not generate any software, except for Perl/bash scripts for subtracting circRNA read counts from the total RNA read count data, which are deposited to https://github.com/pch-code/circ-scripts. Sequencing data are not publicly available due to consent restrictions. Upon request, the data can be made available via controlled access (National Register for Congenital Heart Defects, Berlin, Germany).

METHOD DETAILS

Study Population

Intraoperative RV tissue was obtained from 19 infants with TOF/PS and RVH (age 2–8 months, mean age 5.4 months , 37% female) and 8 age-matched, non-RVH control infants with ventricular septal defects (VSD; 2–12 months, mean age 6 months, 63% female), undergoing open heart surgery for repair of the underlying congenital heart disease. Samples were shock-frozen in liquid nitrogen and stored in the gas phase of liquid nitrogen at -160°C. Written informed consent was obtained as appropriate.

Tissue samples were obtained from the Biobank of the National Registry for Congenital Heart Defects, a repository for medical data and samples from patients with congenital heart defects in Germany. The collection of samples and use for research studies has been approved by the Ethics Committees of the Medical Faculty of the Berlin Charité (EA2/131/10), and Hannover Medical School (#3239-2016). The study included patients (age range 2 - 12 months) who underwent open-heart surgery with routine removal of residual RV or RVOT tissue. All cardiac surgeries were clinically indicated.

Human cardiac tissue samples and RNA-seq data were handled anonymously and with informed consent of the legal caregivers of the patients, according to the principles expressed in the Declaration of Helsinki. The specific CNCHD (KNAHF) project number is 2014-BB-01 (PI: G. Hansmann)

Sample Preparation

The collected tissue subjected to further RNA extraction was pre-treated with RNAlater®-ICE Frozen Tissue Transition Solution (Ambion) and stored at -80°C. Human RV tissue (10-50 mg) was subjected to a tissue grinder and then used for

total RNA and miRNA extraction according to the TRIzol protocol (TRIzol, Life Technologies; 1mL/sample). The samples passed the quality control requirements necessary for total RNA sequencing as specified by Beijing Genomics Institute (BGI) (RIN≥7.0, c≥20ng/μl, 28S/18S≥1.0).

RNA-Sequencing

RNA-Sequencing was performed by BGI, following their ribosomal depletion protocol. TruSeq transcriptome libraries were prepared for each sample following established protocols from Illumina and then sequenced on HiSeq4000 producing 100bp paired-end reads (at least 10Gb of clean data per sample) for total RNA libraries and 20 million 50bp single-end reads for miRNA libraries.

QUANTIFICATION AND STATISTICAL ANALYSIS

Differential RNA expression analysis

mRNA expression levels were estimated using the total RNA-seq protocol depleting the ribosomal RNA and amplifying fragments >200 bp. Illumina reads were aligned to the human genome (GRCh38) using STAR(Dobin et al., 2013) and the read counts corresponding to the Ensembl-annotated genes were identified using RSEM.(Li and Dewey, 2011) CircRNAs were identified using STARChip (https://starchip.readthedocs.io/en/latest/). We used an in-house pipeline to estimate circRNA read counts and subtract them from the total RNA read alignment data. The Perl and bash scripts were deposited to https://github.com/pch-code/circ-scripts. CircRNA expression was estimated based on the read counts in the chimeric junctions and the length of the corresponding circRNA. Therefore, the absolute

expression only provides our best estimate. On the other hand, differential expression of the circRNA isoforms that we report here is based on application of the same approximation method to both cases and controls, and most likely accurately represents actual fold changes of differential expression. Differential gene expression was analyzed using DEseq(Anders and Huber, 2010) after within-lane GC normalization by EDAseq.(Risso et al., 2011) The sharing mode parameter was set to "fit-only" for the estimateDispersions method in DESeq. Benjamini-Hochberg false discovery rate (FDR) procedure was applied to correct for multiple testing. Additionally, the gene filtering procedure developed by Bourgon et al.(Bourgon et al., 2010) was applied to improve the detection power. RNAs with FDR-adjusted P values < 0.05 were considered significantly differentially expressed.

Of note, interpretation of the transcriptional effects of RVH in the older group (TOF/PS vs. VSD in 7-8 month old patients) in our study was somewhat confounded by sex effect, since in this older age group we have 25% males in VSD and 60% males in TOF/PS. To mitigate this data imbalance and to account for age and sex differences in RVH adaptation, we removed genes identified as affected by sex (regulated in the same direction) in both TOF/PS and VSD groups in male vs. female comparisons. Age specific genes were also removed if they were regulated in the same direction in both TOF/PS and VSD groups in the older (7-8 months) vs. younger (2-4 months) comparisons.

Construction of Competing Endogenous RNA Interaction Networks

To map the expected regulatory sponging effects of circRNA and lncRNA on the miRNA, we used the identified differentially expressed sets of these RNA classes. TargetScan 7.1(Agarwal et al., 2015) was applied to identify the circRNA and lncRNA

targets based on the number of occurrences of matching 6-mers, 7-mers, and 8-mers. The affinity score was calculated as Score = 0.43* N_{8mer_1a} + 0.25* N_{7mer_m8} + 0.19* N_{7mer_1a} + 0.07* $N_{6mer.}$ Here, 8mer_1a is a site with an exact match to positions 2-8 of the mature miRNA (the seed) followed by an 'A', 7mer_m8 is a site with exact match to positions 2-8 of the mature miRNA (the seed + position 8), 7mer_1a is a site with an exact match to positions 2-7 of the mature miRNA (the seed) followed by an 'A', 6mer is a site with an exact match to positions 2-6 of the mature miRNA (the seed + position 6) followed by an 'A'. All matches with the score ≥ 1 were considered significant. We used miRDB(Chen and Wang, 2020) as the source of gene targets, considering all targets with the miRDB Target Score ≥ 50 as significant. The epigenetic regulation networks joining the targets of the differentially expressed miRNAs were constructed using Cytoscape.(Shannon et al., 2003)

Pathway and GO overrepresentation analysis

Pathway and GO overrepresentation analyses based on lists of DEGs were performed using the online resource called Enrichr(Chen et al., 2013) with the NCATS BioPlanet pathway annotation (https://ncats.nih.gov/pubs/features/bioplanet). The overrepresentation analysis was based on Fisher exact test and correction of the resulting p-values for multiple testing as implemented in Enrichr. Pathways with the adjusted p-value < 0.05 were considered significantly overrepresented by DEGs.

Co-expression analysis

To identify hub molecules driving RVH-related biological processes, we employed co-expression analysis that included all classes of differentially expressed RNA. The input data consisted of variance-stabilized counts of differentially expressed mRNA, lncRNA, miRNA, and circRNA that were processed using the partial correlation coefficient with information theory (PCIT) approach as implemented in the PCIT R package(Watson-Haigh et al., 2010) to identify informative correlations. The resulting adjacency matrix was converted to a dissimilarity matrix for building co-expression graphs in a form of minimum spanning trees (MST), in which connections between less correlated molecules were removed to avoid cycles in the graph. In such a graph, a hub molecule with all its (highly correlated) direct neighbors, likely represents a transcriptionally regulated biological process. This analysis was performed separately for TOF/PS (RVH) data and VSD (no RVH) control data. Within the produced MSTs, we identified several “hub” genes with the out-degree ≥ 7, i.e., having at least seven direct neighbors. These clusters of DEGs were further expanded to include any neighboring DEGs with the dissimilarity distance measure within 0.05. The co-expression network analysis was performed only for the entire

cohort, because the subgroups had fewer DEGs and failed to produce meaningful co-expression networks.

EXTENDED DISCUSSION

We conducted the first study of human RV hypertrophy by means of comprehensive RNA expression and RNA interaction network analysis, including predicted sponging of miRNA by circRNA and lncRNA. Indeed, we delineated gene expression and transcript interaction differences specific to age (from two to eight months) and sex. While the gene expression profiles were most consistent in males and the youngest infants (2-4 months), more divergent expression was observed in females and in older infants (7-8 months) (**Fig. 1**). In line with our findings, sexually dimorphic gene expression response to Angiotensin II induced cardiac fibrosis was reported in mice, in all cardiac tissue types.(McLellan et al., 2020)

Previous human RVH RNA expression studies relied on postmortem controls to study mRNA expression (Gene Expression Omnibus accession GSE26125 (Bittel et al., 2011; Yang et al., 2013) and GSE 35776 (O'Brien et al., 2012; Wang et al., 2014)) and expression of miRNA (accession GSE40128 (Zhang et al., 2013)), and expression of miRNA and small no-non coding RNA (accession GSE35490 (Bittel et al., 2014; O'Brien et al., 2012; Wang et al., 2014)). Therefore, the results of these studies cannot be used for direct comparison with our data (intraoperative, freshly snap frozen RV tissue). Moreover, all these studies used micro array panels, further complicating possible comparison with our RNA-seq results. For example, we identified 528 DEGs (before subtraction of age- and sex-specific DEGs) in human compensated RVH (cRVH, here: TOF/PS) vs. controls (VSD), compared to 2,274 DEGs (Yang et al., 2013) in the dataset with postmortem controls that was used in both Bittel et al. (Bittel et al., 2011) and Yang et al. (Yang et al., 2013).

On the mRNA level, after accounting for age- and sex-specific genes, we found that the DEGs involved in RVH were overrepresented in pathways related to

TGFβ- and IL-1 regulation of ECM, IL-4- and FSH regulation of apoptosis, ECM-receptor interaction, oncostatin M, beta-1 integrin cell surface interactions, RAGE pathway, focal adhesion, collagen biosynthesis, and integrins in angiogenesis, among others (**Supplementary File 1**). Some of these pathways have been reported to be involved in cardiac hypertrophy, as further discussed below.

TGFβ- and regulation of ECM

The role of TGFβ in induction of fibrosis and cardiac remodeling is well known (reviewed in (Dobaczewski et al., 2011)). In the male rabbit PA banding model, TGFβ mRNA was substantially increased in both RV and LV, resulting in biventricular hypertrophy, fibrosis, and apoptosis.(Friedberg et al., 2013) In monocrotaline-treated rats, SU5416/hypoxia-treated rats, and SU5416/hypoxia-treated mice, selective TGFβ ligand blockade improved hemodynamics and RVH remodeling.(Yung et al., 2016)

IL-1 regulation of ECM

IL-1β was shown to induce cardiac fibrosis by stimulation of rat cardiac fibroblast migration via MAP kinase pathways.(Mitchell et al., 2007)

Integrins

Binding of integrins to ECM ligands results in initiation of protein signaling in various pathways involved in cardiac hypertrophy, e.g., AKT, JNK, ERK, and P38.(Israeli-Rosenberg et al., 2014)

Focal adhesion

Focal adhesion integrity in response to biomechanical stress in cardiomyocytes is modulated by focal adhesion kinase (FAK), which provides proper response to hypertrophic stimuli. Cardiomyocyte-specific deletion of FAK in mice increased LV

chamber dimensions, the heart/body weight ratio, and the expression of markers of cardiac hypertrophy.(Peng et al., 2006)

Oncostatin M

Oncostatin M is a cytokine that belongs to the IL-6 class of cytokines and acts as a major mediator of cardiomyocyte remodeling.(Kubin et al., 2011) Inhibition of oncostatin M in a dilated LV cardiomyopathy mouse model improved cardiac performance.(Kubin et al., 2011)

RAGE pathway

Receptor for advanced glycation end products (RAGE) is a pattern recognition receptor (PRR) that is activated in necrotic cardiomyocytes, which initiates a pro-inflammatory cascade.(Haque and Wang, 2017) We have previously shown that hypoxia drives cardiac miRNAs and inflammation in the right and left ventricle.(Chouvarine et al., 2019) Consistently, hypoxic $Rage^{-/-}$ mice developed less RVH compared to hypoxic wild type mice.(Bauer et al., 2013)

Apoptosis, fibrosis, accumulation of collagens

Cardiomyocyte apoptosis, fibrosis, and accumulation of collagens contribute to the transition from compensated to decompensated cardiac hypertrophy. (Tham et al., 2015)

Another important finding in our current study on compensated RVH (in the “All” group), is upregulation of FABP4, a fatty acid binding protein known to positively regulate cardiac hypertrophy via activation of the ERK signal pathway.(Zhang et al., 2016). Consistently, we had previously demonstrated FABP4 downregulation to be evident in the RV of end-stage PH patients with decompensated RVH(Legchenko et al., 2018), and FABP4 induction by the PPARγ agonist pioglitazone that was

associated with reversal of both RV dysfunction and severe PH in Sugen-hypoxia exposed rats (Legchenko et al., 2018).

On the non-coding RNA level, we report for the first time miRNAs, lncRNAs, and circRNAs associated with human RVH (**Tables S2-S4**). To our knowledge, previous reports identified several miRNAs associated with either LVH,(Mohan et al., 2018; Rau et al., 2017; Wehbe et al., 2019) RVH in rodent pulmonary artery (PA) banding models (Andersen et al., 2020; Reddy and Bernstein, 2015; Reddy et al., 2012; Thum and Batkai, 2014), or human RVH with postmortem control samples.(Bittel et al., 2014; O'Brien et al., 2012; Wang et al., 2014; Zhang et al., 2013) None of the previously reported miRNAs in cardiac hypertrophy of animals or humans were found in our human RVH study, with the exception of miR-216a and miR-217, which were downregulated in human cRVH in our study. MiR-216a has been reported as significantly upregulated in LV of decompensated cardiac myopathy patients and significantly downregulated in human fetal LV.(Akat et al., 2014) Reactivation of a fetal miRNA program and the corresponding alterations in gene expression are known to play a significant role in human cardiac hypertrophy and heart failure.(Wang and Yang, 2012) Thus, downregulation of miR-216a in our study is in line with postnatal fetal gene programming that we hypothesized to occur in infants with RVH. MiR-217 (downregulated in our study) was slightly upregulated in mouse models of thoracic aortic banding- and calcineurin-A-induced LV hypertrophy using miRNA microarrays; however, its upregulation could not be validated by Northern blot analysis.(van Rooij et al., 2006) Another study(Nie et al., 2018) claimed that elevated levels of miR-217 in a mouse transverse aortic constriction (TAC) model of LVH are pro-hypertrophic by targeting PTEN; however, PTEN is not listed as a target of miR-217 in either mirDB(Chen and Wang, 2020) or Targetscan database(Agarwal et al., 2015) (neither for mouse nor human). Additionally, in *in vitro*

and aortic banding rat model of LVH, H3K9me2 was reduced via a miR-217-mediated decrease in expression of the H3K9 dimethyltransferases EHMT1 and EHMT2 (loss of H3K9me2 was shown to be associated with pathologic hypertrophy).(Thienpont et al., 2017) Thus, upregulation of miR-217 in our study either is a protective response or may reflect the differences in rodent LVH vs. human RVH expression differences.

lncRNAs can modulate gene expression via several mechanisms (signaling induced by transcription factors, miRNA sponging, recruiting chromatin-modifying enzymes, and molecular scaffolding resulting in histone modification).(Wang and Chang, 2011) Within the scope of our study, we could concentrate on the decoy function (miRNA sponging) of lncRNAs. Reportedly, Mhrt, Chast, CHRF, ROR, H19, Plscr4, and MIAT are associated with cardiac hypertrophy, and MALAT1, wisper, MEG3, and H19 are involved in ECM remodeling (reviewed in (Zhou et al., 2019) and (Liu and Tang, 2019)). Additionally, Uca1(Zhou et al., 2018) and Peg10(Wen et al., 2019) have been reported as modulators of LVH via Hoxa9 in mouse TAC models. While Kcnq1ot1 was shown to sequester miR-30e-5p to release Adam9 thereby inducing cardiac hypertrophy in Angiotensin II-stimulated hypertrophic cardiomyocyte cell culture.(Wang et al., 2020)

Aside from the H19 studies discussed below, the above-mentioned lncRNAs were identified in LV studies that used either TAC mouse models of LVH, LV tissue from ischemic cardiomyopathy patients and controls, or coronary ligation ischemia mouse models.(Zhou et al., 2019) From the above list of lncRNAs compiled from the published literature on LVH, MEG3 and KCNQ1OT1 were found to be significantly downregulated in our study. The lncRNA KCNQ1OT1 was downregulated (fold change 0.75) in our study (human RVH) and predicted to sponge miR-371 and miR-

372a, both of which target PTEN, a known suppressor of the PI3K/AKT/cardiac-hypertrophy axis.(Aoyagi and Matsui, 2011) Thus, lower expression levels of KCNQ1OT1 in human RVH suggest an alternative decoy function of this lncRNA compared to the one observed in cardiomyocyte cell culture.(Wang et al., 2020) Of note, aside from its decoy function, KCNQ1OT1 is known to accumulate at promoter chromatin of silenced alleles thereby mediating repressive histone modifications.(Wang and Chang, 2011) Whether this histone modifying function of KCNQ1OT1 plays any role in human RVH, warrants further investigation.

In ECM remodeling, cardiac fibroblasts produce various types of matrix metalloproteinases (MMPs). In a mouse transverse aortic constriction (TAC) model of LV pressure overload, silencing lncRNA Meg3 suppressed the induction of Mmp-2 by TGFβ.(Piccoli et al., 2017) . The downregulation of MEG3 that we found in our study (fold change 0.69) may drive RVH via the consecutive reduced sponging of miR-371a that is predicted to inhibit anti-hypertrophic PTEN, leading to disinhibition of pro-hypertrophic PI3K/AKT (**Fig. 2**). Whether MEG3 affects induction of MMP-2 in human RVH should be investigated in future studies.

Interestingly, a recent study used targeted quantitative PCR of RV biopsies of end-stage PH patients and postmortem or aortic valve stenosis controls, to show that H19 is upregulated in decompensated RVH.(Omura et al., 2020) The role of lncRNA H19 in decompensated cardiac hypertrophy appears to be either ventricle-specific, not conserved among species, or ambiguous: H19 was found to be induced in decompensated human RVH,(Omura et al., 2020) but decreased in the decompensated, hypertrophied and failing LV in a pig LVH model.(Viereck et al., 2020) Our study subjects (TOF/PS) had adaptive, compensated RVH without RV failure, and H19 was slightly upregulated (fold change 1.17), but not differentially

expressed (q-value 0.56) in the overall cohort. In failure applied rodent RV pressure load models (monocrotaline, PA-banding), H19 RV mRNA expression progressively increased (from compensated to decompensated state).(Omura et al., 2020) We speculate that H19 in humans also becomes progressively upregulated as RVH transitions to the decompensated state, in line with our findings and the results published by Omura et al.(Omura et al., 2020)

To our knowledge, presently there are no published circRNA studies on human RVH. In a mouse TAC LVH study, circSlc8a1 was implicated as a sponge of miR-133a, an anti-hypertrophic miRNA in the context of LVH.(Lim et al., 2019) In our study, circSLC8A1 was upregulated seven fold in the older female group (TOF/PS vs control). However, while miR-133a was not detected in this group, miR-133b (known as a possible suppressor of cardiac remodeling(Li et al., 2018)) and also targeting circSLC8A1, was downregulated (fold change 0.59), though not significantly.

In our circ/lncRNA-miRNA-mRNA interaction network (**Fig. 2A**) RVH-associated miRNAs targeting key cardiac hypertrophy genes appear to have the most sponging circ/lncRNA regulators/decoys. Clearly regulated key genes (**Fig. 2A**) include: PTEN downregulated by combined action of miR-372A (with five ncRNA decoys) and miR-371 (with three ncRNA decoys); PDK1 and MSK1 upregulated by miR-216A (with eight ncRNA decoys); and GSK3B, PI3KP1, and FOXO3 upregulated by miR-5008 (with six ncRNA decoys). Such heavy reliance on epigenetic regulation indicate that the known pro-hypertrophic pathways enabled by these genes (PTEN, PDK1, GSK3B,(Dorn and Force, 2005) MSK1,(Markou et al., 2009) PI3KIP1,(Song et al., 2015) and FOXO3(Ni et al., 2006)) are particularly important in human cRVH.

Gene co-expression analysis gave us another way to gain insight into key biological processes in human RVH. While most pathways overrepresented in co-

expressed DEG clusters were also identified in our differential gene expression analysis, we also found significantly overrepresented pathways related to *1)* small leucine-rich proteoglycan (SLRP) molecules (BGN and FMOD); *2)* cell adhesion molecules (CAMs; CLDN11, VCAN, NLGN2, ITGA8, NRXN2, NRCAM); *3)* keratan sulfate/keratin metabolism (ACAN, CHST6, FMOD, CHST2); and *4)* inflammatory response (COL1A2, FN1, THBS3). Biglycan (BGN) is one of SLRPs involved in ECM remodeling by regulating both collagen amount and fibrillogenesis in the heart.(Andenaes et al., 2018) Bgn deficiency was shown to promote differentiation of cardiac fibroblasts into myofibroblasts and their further proliferation, likely as an increased response to TGFβ and Smad2 signaling.(Melchior-Becker et al., 2011) In our study, BGN was downregulated in human RVH, probably resulting in a pro-fibrotic state. Fibromodulin (FMOD) is a collagen-binding keratan sulfate SLRP. Increased expression of Fmod in cardiac fibroblasts reduced the expression of transglutaminase 2 and periostin, both of which are known to induce cardiac fibrosis.(Andenaes et al., 2018) In our data, FMOD was downregulated in RVH, thereby likely contributing to fibrosis.

The strength of our study is the first comprehensive view of transcriptomic expression in human RVH *in vivo*. To the best of our knowledge, ours is the first study exploring lncRNA and circRNA expression, as well as miRNAs, in human RVH. This is particularly important since lncRNA and circRNA have poor species conservation, so that cell culture and animal studies are difficult to translate to human diseases. However, our study has certain limitations: Due to the large volume of data, the regulatory mechanisms that we present are based largely on *in silico* predictions - their validation will need to be conducted in subsequent research. Because cardiac surgery on the TOF/PS (cRVH) and VSD (control) patients had to be performed within the first year of life, our findings may not fully reflect RVH in older patients.

However, we did exclude neonates (first postnatal month) and performed subgroup analyses by age and sex. Finding non-surgical human RVH and non-RVH samples for a representative *in vivo* study is difficult (ethics, consent), but has been pursued in adults with scleroderma-associated or idiopathic PH, via RV septal endomyocardial biopsies.(Hsu et al., 2018) Recently, a specific RNA signature of tissue fibrosis and enrichment of beneficial metabolic regulators (AMPK, PPARs) was identified in animal models for fibrosis: kidney, liver and lung(Zhang et al., 2020) and the failing RV in severe PH.(Legchenko et al., 2018) It has been postulated that mild to moderate fibrosis prevents dilation (cardiomyocyte overstretch) of the hypertrophied ventricles.(Andersen et al., 2019) We found only a moderate induction of a pro-fibrosis mRNA signature in the hypertrophied RV of TOF/PS patients (downregulation of BGN and FMOD), probably because of the high adaptivity and plasticity of the infant myocardium, and the rather short duration of high pressure afterload.

Taken together, we provide RNA expression profiles, signaling characteristics and network analysis of human RVH with high pressure afterload (but no RV failure). The miRNAs reported here are at the core of this transcriptomic regulation in compensated (adaptive) RVH and, as such, are promising targets of heart failure therapies and/or biomarkers of disease severity/progression. Validation of the predicted competing endogenous RNA interactions (sponging of miRNA by circRNA and lncRNA) and further investigation of the regulatory mechanisms should be a focus of future research.

NON-STANDARD ABBREVIATIONS

BDNF, brain-derived neurotrophic factor

CAM, cell adhesion molecule

ceRNA, competing endogenous RNA

circRNA, circular RNA

cRVH, compensated right-ventricular hypertrophy

DEG, differentially expressed genes

ECM, extracellular matrix

FDR, false discovery rate

lncRNA, long non-coding RNA

LVH, left-ventricular hypertrophy

miRNA, micro RNA

MST, minimum spanning tree

PS, pulmonary stenosis

RVH, right-ventricular hypertrophy

SLRP, small leucine-rich proteoglycan

TAC, transverse aortic constriction

TOF, tetralogy of Fallot

VSD, ventricular septal defect

KEY RESOURCES TABLE

REAGENT or RESOURCE	SOURCE	IDENTIFIER
Antibodies		
N/A		
Bacterial and Virus Strains		
N/A		
Biological Samples		
Human RV tissue (10-50 mg) was used for total RNA and miRNA extraction according to the TRIzol protocol (TRIzol, Life Technologies).	Hannover Medical School (This study)	N/A
Chemicals, Peptides, and Recombinant Proteins		
N/A		
Critical Commercial Assays		
RNAlater®-ICE Frozen Tissue Transition Solution	Ambion	Cat. No. AM7030
TRIzol™ Reagent	Invitrogen	Cat. No. 15596026
Deposited Data		
Total RNA sequencing	This manuscript	Will be deposited to NCBI SRA upon acceptance
miRNA sequencing	This manuscript	Will be deposited to NCBI SRA upon acceptance
Experimental Models: Cell Lines		
N/A		
Experimental Models: Organisms/Strains		
N/A		
Oligonucleotides		
N/A		
Recombinant DNA		
N/A		
Software and Algorithms		
STAR	(Dobin et al., 2013)	https://github.com/alexdobin/STAR
RSEM	(Li and Dewey, 2011)	https://deweylab.github.io/RSEM/
STARChip	Unpublished	https://starchip.readthedocs.io/en/latest/
Cytoscape	(Shannon et al., 2003)	https://cytoscape.org/
DESeq R package	(Anders and Huber, 2010)	https://bioconductor.org/packages/release/bioc/html/DESeq.html
EDASeq R package	(Risso et al., 2011)	https://bioconductor.org/packages/release/bioc/html/EDASeq.html
Gene filtering procedure to increase detection power of differential expression analysis	(Bourgon et al., 2010)	https://www.pnas.org/content/107/21/9546
PCIT R package	(Watson-Haigh et al., 2010)	https://cran.r-project.org/src/contrib/Archive/PCIT/

Enrichr	(Chen et al., 2013)	https://amp.pharm.mssm.edu/Enrichr/
RNAInter	(Lin et al., 2020)	http://www.rna-society.org/rnainter/
TargetScan 7.1	(Agarwal et al., 2015)	http://www.targetscan.org/vert_71/
miRDB	(Chen and Wang, 2020)	http://mirdb.org/index.html
Perl scripts for subtraction of circRNA counts from total RNA	This manuscript	https://github.com/pch-code/circ-scripts
Other		
N/A		

SUPPLEMENTAL REFERENCES

Agarwal, V., Bell, G.W., Nam, J.W., and Bartel, D.P. (2015). Predicting effective microRNA target sites in mammalian mRNAs. Elife 4, e05005.

Akat, K.M., Moore-McGriff, D., Morozov, P., Brown, M., Gogakos, T., Correa Da Rosa, J., Mihailovic, A., Sauer, M., Ji, R., Ramarathnam, A., *et al.* (2014). Comparative RNA-sequencing analysis of myocardial and circulating small RNAs in human heart failure and their utility as biomarkers. Proc Natl Acad Sci U S A 111, 11151-11156.

Andenaes, K., Lunde, I.G., Mohammadzadeh, N., Dahl, C.P., Aronsen, J.M., Strand, M.E., Palmero, S., Sjaastad, I., Christensen, G., Engebretsen, K.V.T., *et al.* (2018). The extracellular matrix proteoglycan fibromodulin is upregulated in clinical and experimental heart failure and affects cardiac remodeling. PLoS One 13, e0201422.

Anders, S., and Huber, W. (2010). Differential expression analysis for sequence count data. Genome Biol 11, R106.

Andersen, A., van der Feen, D., Andersen, S., Schultz, J., Hansmann, G., and Bogaard, H. (2020). Animal models of right heart failure. Cardiovasc Diagn Ther 10, 1561-1579.

Andersen, S., Nielsen-Kudsk, J.E., Vonk Noordegraaf, A., and de Man, F.S. (2019). Right Ventricular Fibrosis. Circulation 139, 269-285.

Aoyagi, T., and Matsui, T. (2011). Phosphoinositide-3 kinase signaling in cardiac hypertrophy and heart failure. Curr Pharm Des 17, 1818-1824.

Bauer, E.M., Shapiro, R., Zheng, H., Ahmad, F., Ishizawar, D., Comhair, S.A., Erzurum, S.C., Billiar, T.R., and Bauer, P.M. (2013). High mobility group box 1 contributes to the pathogenesis of experimental pulmonary hypertension via activation of Toll-like receptor 4. Mol Med 18, 1509-1518.

Bittel, D.C., Butler, M.G., Kibiryeva, N., Marshall, J.A., Chen, J., Lofland, G.K., and O'Brien, J.E., Jr. (2011). Gene expression in cardiac tissues from infants with idiopathic conotruncal defects. BMC Med Genomics 4, 1.

Bittel, D.C., Kibiryeva, N., Marshall, J.A., and O'Brien, J.E. (2014). MicroRNA-421 Dysregulation is Associated with Tetralogy of Fallot. Cells 3, 713-723.

Bourgon, R., Gentleman, R., and Huber, W. (2010). Independent filtering increases detection power for high-throughput experiments. Proc Natl Acad Sci U S A 107, 9546-9551.

Chen, E.Y., Tan, C.M., Kou, Y., Duan, Q., Wang, Z., Meirelles, G.V., Clark, N.R., and Ma'ayan, A. (2013). Enrichr: interactive and collaborative HTML5 gene list enrichment analysis tool. BMC Bioinformatics 14, 128.

Chen, Y., and Wang, X. (2020). miRDB: an online database for prediction of functional microRNA targets. Nucleic Acids Res 48, D127-D131.

Chouvarine, P., Legchenko, E., Geldner, J., Riehle, C., and Hansmann, G. (2019). Hypoxia drives cardiac miRNAs and inflammation in the right and left ventricle. J Mol Med (Berl) 97, 1427-1438.

Dobaczewski, M., Chen, W., and Frangogiannis, N.G. (2011). Transforming growth factor (TGF)-beta signaling in cardiac remodeling. J Mol Cell Cardiol 51, 600-606.

Dobin, A., Davis, C.A., Schlesinger, F., Drenkow, J., Zaleski, C., Jha, S., Batut, P., Chaisson, M., and Gingeras, T.R. (2013). STAR: ultrafast universal RNA-seq aligner. Bioinformatics 29, 15-21.

Dorn, G.W., 2nd, and Force, T. (2005). Protein kinase cascades in the regulation of cardiac hypertrophy. J Clin Invest 115, 527-537.

Friedberg, M.K., Cho, M.Y., Li, J., Assad, R.S., Sun, M., Rohailla, S., Honjo, O., Apitz, C., and Redington, A.N. (2013). Adverse biventricular remodeling in isolated right ventricular hypertension is mediated by increased transforming growth factor-beta1 signaling and is abrogated by angiotensin receptor blockade. Am J Respir Cell Mol Biol 49, 1019-1028.

Haque, Z.K., and Wang, D.Z. (2017). How cardiomyocytes sense pathophysiological stresses for cardiac remodeling. Cell Mol Life Sci 74, 983-1000.

Hsu, S., Kokkonen-Simon, K.M., Kirk, J.A., Kolb, T.M., Damico, R.L., Mathai, S.C., Mukherjee, M., Shah, A.A., Wigley, F.M., Margulies, K.B., *et al.* (2018). Right Ventricular Myofilament Functional Differences in Humans With Systemic Sclerosis-Associated Versus Idiopathic Pulmonary Arterial Hypertension. Circulation 137, 2360-2370.

Israeli-Rosenberg, S., Manso, A.M., Okada, H., and Ross, R.S. (2014). Integrins and integrin-associated proteins in the cardiac myocyte. Circ Res 114, 572-586.

Kubin, T., Poling, J., Kostin, S., Gajawada, P., Hein, S., Rees, W., Wietelmann, A., Tanaka, M., Lorchner, H., Schimanski, S., *et al.* (2011). Oncostatin M is a major mediator of cardiomyocyte dedifferentiation and remodeling. Cell Stem Cell 9, 420-432.

Legchenko, E., Chouvarine, P., Borchert, P., Fernandez-Gonzalez, A., Snay, E., Meier, M., Maegel, L., Mitsialis, S.A., Rog-Zielinska, E.A., Kourembanas, S., *et al.* (2018). PPARgamma agonist pioglitazone reverses pulmonary hypertension and prevents right heart failure via fatty acid oxidation. Sci Transl Med 10, eaao0303.

Li, B., and Dewey, C.N. (2011). RSEM: accurate transcript quantification from RNA-Seq data with or without a reference genome. BMC Bioinformatics 12, 323.

Li, N., Zhou, H., and Tang, Q. (2018). miR-133: A Suppressor of Cardiac Remodeling? Front Pharmacol 9, 903.

Lim, T.B., Aliwarga, E., Luu, T.D.A., Li, Y.P., Ng, S.L., Annadoray, L., Sian, S., Ackers-Johnson, M.A., and Foo, R.S. (2019). Targeting the highly abundant circular RNA circSlc8a1 in cardiomyocytes attenuates pressure overload induced hypertrophy. Cardiovasc Res 115, 1998-2007.

Lin, Y., Liu, T., Cui, T., Wang, Z., Zhang, Y., Tan, P., Huang, Y., Yu, J., and Wang, D. (2020). RNAInter in 2020: RNA interactome repository with increased coverage and annotation. Nucleic Acids Res 48, D189-D197.

Liu, C.F., and Tang, W.H.W. (2019). Epigenetics in Cardiac Hypertrophy and Heart Failure. JACC Basic Transl Sci 4, 976-993.

Markou, T., Cieslak, D., Gaitanaki, C., and Lazou, A. (2009). Differential roles of MAPKs and MSK1 signalling pathways in the regulation of c-Jun during phenylephrine-induced cardiac myocyte hypertrophy. Mol Cell Biochem 322, 103-112.

McLellan, M.A., Skelly, D.A., Dona, M.S.I., Squiers, G.T., Farrugia, G.E., Gaynor, T.L., Cohen, C.D., Pandey, R., Diep, H., Vinh, A., *et al.* (2020). High-Resolution Transcriptomic Profiling of the Heart During Chronic Stress Reveals Cellular Drivers of Cardiac Fibrosis and Hypertrophy. Circulation 142, 1448-1463.

Melchior-Becker, A., Dai, G., Ding, Z., Schafer, L., Schrader, J., Young, M.F., and Fischer, J.W. (2011). Deficiency of biglycan causes cardiac fibroblasts to differentiate into a myofibroblast phenotype. J Biol Chem 286, 17365-17375.

Mitchell, M.D., Laird, R.E., Brown, R.D., and Long, C.S. (2007). IL-1beta stimulates rat cardiac fibroblast migration via MAP kinase pathways. Am J Physiol Heart Circ Physiol 292, H1139-1147.

Mohan, N., Kumar, V., Kandala, D.T., Kartha, C.C., and Laishram, R.S. (2018). A Splicing-Independent Function of RBM10 Controls Specific 3' UTR Processing to Regulate Cardiac Hypertrophy. Cell reports 24, 3539-3553.

Ni, Y.G., Berenji, K., Wang, N., Oh, M., Sachan, N., Dey, A., Cheng, J., Lu, G., Morris, D.J., Castrillon, D.H., *et al.* (2006). Foxo transcription factors blunt cardiac hypertrophy by inhibiting calcineurin signaling. Circulation 114, 1159-1168.

Nie, X., Fan, J., Li, H., Yin, Z., Zhao, Y., Dai, B., Dong, N., Chen, C., and Wang, D.W. (2018). miR-217 Promotes Cardiac Hypertrophy and Dysfunction by Targeting PTEN. Mol Ther Nucleic Acids 12, 254-266.

O'Brien, J.E., Kibiryeva, N., Zhou, X.G., Marshall, J.A., Lofland, G.K., Artman, M., Chen, J., and Bittel, D.C. (2012). Noncoding RNA Expression in Myocardium From Infants With Tetralogy of Fallot. Circ-Cardiovasc Gene 5, 279-286.

Omura, J., Habbout, K., Shimauchi, T., Wu, W.H., Breuils-Bonnet, S., Tremblay, E., Martineau, S., Nadeau, V., Gagnon, K., Mazoyer, F., *et al.* (2020). Identification of Long Noncoding RNA H19 as a New Biomarker and Therapeutic Target in Right Ventricular Failure in Pulmonary Arterial Hypertension. Circulation 142, 1464-1484.

Peng, X., Kraus, M.S., Wei, H., Shen, T.L., Pariaut, R., Alcaraz, A., Ji, G., Cheng, L., Yang, Q., Kotlikoff, M.I., *et al.* (2006). Inactivation of focal adhesion kinase in cardiomyocytes promotes eccentric cardiac hypertrophy and fibrosis in mice. J Clin Invest 116, 217-227.

Piccoli, M.T., Gupta, S.K., Viereck, J., Foinquinos, A., Samolovac, S., Kramer, F.L., Garg, A., Remke, J., Zimmer, K., Batkai, S., *et al.* (2017). Inhibition of the Cardiac Fibroblast-Enriched lncRNA Meg3 Prevents Cardiac Fibrosis and Diastolic Dysfunction. Circ Res 121, 575-583.

Rau, C.D., Romay, M.C., Tuteryan, M., Wang, J.J., Santolini, M., Ren, S., Karma, A., Weiss, J.N., Wang, Y., and Lusis, A.J. (2017). Systems Genetics Approach Identifies Gene Pathways and Adamts2 as Drivers of Isoproterenol-Induced Cardiac Hypertrophy and Cardiomyopathy in Mice. Cell Syst 4, 121-128 e124.

Reddy, S., and Bernstein, D. (2015). Molecular Mechanisms of Right Ventricular Failure. Circulation 132, 1734-1742.

Reddy, S., Zhao, M., Hu, D.Q., Fajardo, G., Hu, S., Ghosh, Z., Rajagopalan, V., Wu, J.C., and Bernstein, D. (2012). Dynamic microRNA expression during the transition from right ventricular hypertrophy to failure. Physiol Genomics 44, 562-575.

Risso, D., Schwartz, K., Sherlock, G., and Dudoit, S. (2011). GC-content normalization for RNA-Seq data. BMC Bioinformatics 12, 480.

Shannon, P., Markiel, A., Ozier, O., Baliga, N.S., Wang, J.T., Ramage, D., Amin, N., Schwikowski, B., and Ideker, T. (2003). Cytoscape: a software environment for integrated models of biomolecular interaction networks. Genome Res 13, 2498-2504.

Song, H.K., Kim, J., Lee, J.S., Nho, K.J., Jeong, H.C., Kim, J., Ahn, Y., Park, W.J., and Kim, D.H. (2015). Pik3ip1 modulates cardiac hypertrophy by inhibiting PI3K pathway. PLoS One 10, e0122251.

Tham, Y.K., Bernardo, B.C., Ooi, J.Y., Weeks, K.L., and McMullen, J.R. (2015). Pathophysiology of cardiac hypertrophy and heart failure: signaling pathways and novel therapeutic targets. Arch Toxicol 89, 1401-1438.

Thienpont, B., Aronsen, J.M., Robinson, E.L., Okkenhaug, H., Loche, E., Ferrini, A., Brien, P., Alkass, K., Tomasso, A., Agrawal, A., *et al.* (2017). The H3K9 dimethyltransferases EHMT1/2 protect against pathological cardiac hypertrophy. J Clin Invest 127, 335-348.

Thum, T., and Batkai, S. (2014). MicroRNAs in right ventricular (dys)function (2013 Grover Conference series). Pulm Circ 4, 185-190.

van Rooij, E., Sutherland, L.B., Liu, N., Williams, A.H., McAnally, J., Gerard, R.D., Richardson, J.A., and Olson, E.N. (2006). A signature pattern of stress-responsive microRNAs that can evoke cardiac hypertrophy and heart failure. Proceedings of the National Academy of Sciences of the United States of America 103, 18255-18260.

Viereck, J., Buhrke, A., Foinquinos, A., Chatterjee, S., Kleeberger, J.A., Xiao, K., Janssen-Peters, H., Batkai, S., Ramanujam, D., Kraft, T., *et al.* (2020). Targeting muscle-enriched long non-coding RNA H19 reverses pathological cardiac hypertrophy. Eur Heart J 41, 3462-3474.

Wang, J., and Yang, X. (2012). The function of miRNA in cardiac hypertrophy. Cell Mol Life Sci 69, 3561-3570.

Wang, K.C., and Chang, H.Y. (2011). Molecular Mechanisms of Long Noncoding RNAs. Mol Cell 43, 904-914.

Wang, W., Wu, C., Ren, L., Bao, Y., Han, Y., Li, C., and Li, Y. (2020). MiR-30e-5p is sponged by Kcnq1ot1 and represses Angiotensin II-induced hypertrophic phenotypes in cardiomyocytes by targeting ADAM9. Exp Cell Res 394, 112140.

Wang, X.M., Zhang, K., Li, Y., Shi, K., Liu, Y.L., Yang, Y.F., Fang, Y., and Mao, M. (2014). Screening miRNA and their target genes related to tetralogy of Fallot with microarray. Cardiol Young 24, 442-446.

Watson-Haigh, N.S., Kadarmideen, H.N., and Reverter, A. (2010). PCIT: an R package for weighted gene co-expression networks based on partial correlation and information theory approaches. Bioinformatics 26, 411-413.

Wehbe, N., Nasser, S.A., Pintus, G., Badran, A., Eid, A.H., and Baydoun, E. (2019). MicroRNAs in Cardiac Hypertrophy. International Journal of Molecular Sciences 20(19), 4714.

Wen, Z.Q., Li, S.H., Shui, X., Tang, L.L., Zheng, J.R., and Chen, L. (2019). LncRNA PEG10 aggravates cardiac hypertrophy through regulating HOXA9. Eur Rev Med Pharmacol Sci 23, 281-286.

Yang, D., Li, J., and Yuan, Z. (2013). Gene expression analysis in cardiac tissues from infants identifies candidate agents for Tetralogy of Fallot. Pediatr Cardiol 34, 1637-1644.

Yung, L.M., Nikolic, I., Paskin-Flerlage, S.D., Pearsall, R.S., Kumar, R., and Yu, P.B. (2016). A Selective Transforming Growth Factor-beta Ligand Trap Attenuates Pulmonary Hypertension. Am J Respir Crit Care Med 194, 1140-1151.

Zhang, J., Chang, J.J., Xu, F., Ma, X.J., Wu, Y., Li, W.C., Wang, H.J., Huang, G.Y., and Ma, D. (2013). MicroRNA deregulation in right ventricular outflow tract myocardium in nonsyndromic tetralogy of fallot. Can J Cardiol 29, 1695-1703.

Zhang, J., Muise, E., Han, S., Kutchukian, P., Costet, P., Zhu, Y., Kan, Y., Zhou, H., Shah, V., and Huang, Y. (2020). Molecular Profiling Reveals a Common Metabolic Signature of Tissue Fibrosis. Cell Rep Med 1, 100056.

Zhang, J., Qiao, C., Chang, L., Guo, Y., Fan, Y., Villacorta, L., Chen, Y.E., and Zhang, J. (2016). Cardiomyocyte Overexpression of FABP4 Aggravates Pressure Overload-Induced Heart Hypertrophy. PLoS One 11, e0157372.

Zhou, G., Li, C., Feng, J., Zhang, J., and Fang, Y. (2018). lncRNA UCA1 Is a Novel Regulator in Cardiomyocyte Hypertrophy through Targeting the miR-184/HOXA9 Axis. Cardiorenal Med 8, 130-139.

Zhou, H., Wang, B., Yang, Y.X., Jia, Q.J., Zhang, A., Qi, Z.W., and Zhang, J.P. (2019). Long Noncoding RNAs in Pathological Cardiac Remodeling: A Review of the Update Literature. BioMed research international 2019, 7159592.